# Berenil Binding to Higher Ordered Nucleic Acid Structures: Complexation with a DNA and RNA Triple Helix†

Daniel S. Pilch, Michael A. Kirolos, and Kenneth J. Breslauer*

*Department of Chemistry, Rutgers−The State University of New Jersey, New Brunswick, New Jersey 08903*

*Received August 9, 1995; Revised Manuscript Received September 29, 1995*⊗

ABSTRACT: Berenil is an antitrypanosomal agent that binds to nucleic acid duplexes. Recently, we reported that this drug can bind to both DNA and RNA duplexes, while exhibiting properties characteristic of both intercalation and groove binding [Pilch, D. S., Kirolos, M. A., Liu, X., Plum, G. E., & Breslauer, K. J. (1995) *Biochemistry 34*, 9962−9976]. In this work, we use spectroscopic, calorimetric, and hydrodynamic techniques to demonstrate that berenil also can bind to DNA and RNA triplexes. Our results reveal the following significant features: (i) Berenil binds to the poly(dA)·2poly(dT) DNA triplex and to the poly(rA)·2poly(rU) RNA triplex without displacing the major groove-bound third strands. (ii) Both berenil-bound triplexes melt via two distinct transitions: initial conversion of the triplex to the duplex state, with the berenil remaining bound, followed by denaturation of the duplex to its component single strands. (iii) The magnitude and even the direction of the impact of berenil binding on the thermal stability of the DNA triplex depends on both the $Na^+$ concentration and the drug binding density (the [base triplet]/[total berenil] ratio). Specifically, at $Na^+$ concentrations $\leq 0.08$ M, the DNA triplex to duplex transition is thermally stabilized, while at $Na^+$ concentrations $\geq 0.125$ M it is thermally destabilized. Between these two salt concentrations, berenil binding either enhances or diminishes the thermal stability of the DNA triplex in a manner that depends on the [base triplet]/[total berenil] ratio. (iv) The effect of berenil binding on the thermal stability of the RNA triplex to duplex equilibrium also depends on the [base triplet]/[total berenil] ratio, having a weakly destabilizing effect on this equilibrium at [base triplet]/[total berenil] ratios $>5$, while thermally stabilizing this equilibrium at [base triplet]/[total berenil] ratios $<5$. (v) The apparent "site sizes" associated with berenil binding to the triplexes range from approximately 1 to 12 base triplets per bound berenil and depend, in part, on the host triplex. One of the site sizes common to both triplexes is consistent with berenil binding to the minor groove. (vi) Berenil exhibits a higher apparent binding affinity for the DNA triplex relative to the RNA triplex. (vii) Viscometric data reveal nonintercalative binding properties when berenil complexes with both triplexes, consistent with a minor groove binding mode. (viii) Berenil binding to either the DNA or the RNA triplex is enthalpically more favorable than berenil binding to the corresponding duplex. (ix) Berenil binding to both triplexes decreases the cooperativity of the triplex to duplex melting event. A comparison between the berenil binding properties of the corresponding duplex and triplex structures reveals "cross-talk" between the minor groove-bound berenil and the major groove-bound third strands. We comment on the impact of such "cross-talk" on the potential use of nucleic acid-binding ligands to modulate the affinities and specificities of third strands for target duplex domains.

The recognition of the potential biological roles and biomedical applications of triplex structures has rekindled interest in the triple-helical form of nucleic acids, as well as in their interactions with nucleic acid-binding ligands [reviewed in Wells et al. (1988), Hélène and Toulmé (1990), Hélène (1991a,b), and Thuong and Hélène (1993)]. The possibility of intramolecular triplex (H-DNA) formation at mirror-repeated polypurine·polypyrimidine tracts in supercoiled plasmids (Lyamichev et al., 1986; Htun & Dahlberg, 1988; Johnston, 1988), coupled with the frequency with which these tracts occur in the regulatory regions of genes (Wells et al., 1988), has highlighted the potential biological significance of triplex structures. Recent applications of triple-stranded structures include the selective control of gene expression at the transcriptional and/or DNA replication level [reviewed in Hélène and Toulmé (1990), Hélène (1991a,b), Thuong and Hélène (1993)] and the mapping of megabase DNA by sequence-specific cleavage of duplex DNA (Moser & Dervan, 1987; François et al., 1989; Perrouault et al., 1990). Controlling the affinity and specificity of third strands for their target duplexes is central to the advancement of such applications. One approach to achieve such control is through the use of nucleic acid-binding ligands to modulate the hybridization of third strands to specific duplex targets. To date, relatively few such studies have been reported. These reports include investigations of the influence of intercalating ligands (Waring, 1974; Lehrman & Crothers, 1977; Bresloff & Crothers, 1981; Scaria & Shafer, 1991; Sun et al., 1991; Mergny et al., 1991, 1992; Pilch et al., 1993a,b; Lee et al., 1993; Wilson et al., 1993) and minor groove-binding ligands (Umemoto et al., 1990; Park & Breslauer, 1992; Durand et al., 1992; Lin & Patel, 1992) on triplex formation. The majority of these studies have

† This work was supported by National Institutes of Health Grants GM23509, GM34469, and CA47995.

* To whom correspondence should be addressed.

⊗ Abstract published in *Advance ACS Abstracts,* December 1, 1995.

0006-2960/95/0434-16107$09.00/0 

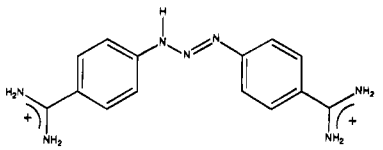

FIGURE 1: Chemical structure of berenil [1,3-*bis*(4′-amidinophenyl)-triazene].

examined the influence on triplex formation of either the intercalating ligand ethidium bromide (Waring, 1974; Lehrman & Crothers, 1977; Bresloff & Crothers, 1981; Scaria & Shafer, 1991; Sun et al., 1991; Mergny et al., 1991) or the minor groove-binding oligopeptide antibiotic netropsin (Park & Breslauer, 1992; Durand et al., 1992). All but three of these studies (Waring, 1974; Lehrman & Crothers, 1977; Bresloff & Crothers, 1981) have probed the influence of ligand binding exclusively on DNA triplex formation. To broaden our base of knowledge of how ligand binding can modulate triplex formation, we have begun a program in which we are characterizing the influences of various nucleic acid-binding ligands on the properties of DNA, RNA, and DNA−RNA hybrid triplexes.

In this work, we characterize the interactions of the antitrypanosomal agent berenil [1,3-*bis*(4′-amidinophenyl)-triazene] (Figure 1) with both a DNA and a RNA triple helix, while examining the influence of berenil binding on the thermal stability, melting energetics, and melting cooperativity of these nucleic acid structures. Our results reveal that berenil exhibits properties characteristic of minor groove-binding when complexed with both classes of triplexes, while providing evidence for cross-talk between the minor groove-bound berenil and the major groove-bound third strands. These results suggest that minor groove-directed ligands can be used to modulate the affinity and/or specificity of major groove-binding third strands in triplex-based therapeutic, diagnostic, and/or biotechnological strategies. Independent of these potential applications, our results provide new information about the drug binding properties of nucleic acid triplexes, while also yielding insight into the cross-talk that can occur between ligands bound in the major and minor grooves of both DNA and RNA double helices.

## MATERIALS AND METHODS

*Nucleic Acid and Drug Molecules.* DNA and RNA polymers were purchased from Pharmacia Biotech, Inc. (Piscataway, NJ) and were used without further purification. These polymers were dissolved in 10 mM sodium cacodylate (pH 6.8) to concentrations of approximately 6−7 mM in nucleotide. The concentrations of all the polymer solutions were determined spectrophotometrically using the following extinction coefficients in units of (mol of nucleotide/L) $^{-1}$ cm$^{-1}$: $\epsilon_{260}$ = 6000 for poly(dA)·poly(dT), $\epsilon_{265}$ = 8700 for poly(dT), $\epsilon_{258}$ = 9800 for poly(rA), and $\epsilon_{260}$ = 9350 for poly(rU). Solutions containing either the poly(rA)·poly(rU) RNA duplex or the poly(rA)·2poly(rU)[1] RNA triplex were prepared by mixing poly(rA) and poly(rU) single strands in either a 1:1 or a 1:2 molar ratio, respectively. Solutions containing the poly(dA)·2poly(dT) DNA triplex were prepared by mixing the poly(dA)·poly(dT) DNA duplex and the poly(dT) single strand in a 1:1 molar ratio. Prior to each experiment, all DNA and RNA solutions were heated to 90 °C and then cooled slowly to room temperature to minimize formation of competing secondary structures. Isothermal mixing experiments (Job, 1928; Riley et al., 1966; Pilch et al., 1990) using the poly(rA) and poly(rU) single strands established the expected 1:1 and 1:2 stoichiometries corresponding to formation of the poly(rA)·poly(rU) RNA duplex and the poly(rA)·2poly(rU) RNA triplex, respectively (Krakauer & Sturtevant, 1968). Similar experiments for the poly(dA)·poly(dT) DNA duplex and the poly(dT) single strand established the expected 1:1 stoichiometry corresponding to formation of the poly(dA)·2poly(dT) DNA triplex (Riley et al., 1966).

Berenil (97% purity) was obtained from Sigma Chemical Co. (St. Louis, MO). Using previously described methods (Pilch et al., 1995), we determined that further purification of the commercially available drug had no impact on our results. Thus, in these studies, berenil was used as received from Sigma, without further purification. Concentrations of berenil solutions were determined spectrophotometrically using an extinction coefficient (in units of M$^{-1}$ cm$^{-1}$) of $\epsilon_{370}$ = 34 400.

*UV Spectrophotometry.* All UV absorbance measurements were performed on a computer-interfaced, dual-beam, Perkin-Elmer model Lambda 4C spectrophotometer equipped with a thermoelectrically controlled cell holder. A quartz cell with a 1 cm path length was used for all the UV studies. Absorbance versus temperature profiles were measured at 260 nm, with a heating rate of 0.1 °C/min. For each optically detected transition, the melting temperature ($T_m$) and the van't Hoff transition enthalpy ($\Delta H_{vH}$) were determined as previously described (Marky & Breslauer, 1987). The RNA solutions were 20 $\mu$M in base triplet and contained 10 mM sodium cacodylate (pH 6.9) and 0.1 mM EDTA. The berenil and NaCl concentrations in these solutions ranged from 0 to 9.2 $\mu$M and 0 to 800 mM, respectively. The DNA solutions were 30 $\mu$M in base triplet and contained 10 mM sodium cacodylate (pH 6.8) and 0.1 mM EDTA. The berenil and NaCl concentrations in these solutions ranged from 0 to 13.8 $\mu$M and 0 to 2.5 M, respectively.

Isothermal optical titrations were performed at 25 °C by incrementally adding aliquots (30−78 $\mu$L) of concentrated nucleic acid polymer solutions (2.5 mM for DNA and 6.5 mM for RNA solutions in base pairs or base triplets) into 1 mL solutions containing either 1.5 $\mu$M (for DNA solutions) or 5 $\mu$M (for RNA solutions) berenil. To correct for light scattering by the polynucleotides in the 300−450 nm region (a nonnegligible correction for the high concentrations of nucleic acid used in these titrations), the same amount of nucleic acid polymer solution was titrated into reference solutions containing the appropriate buffer. After each addition, absorbance spectra were recorded from 300 to 450 nm. In these titrations, data points were recorded at [base pair or base triplet]/[total berenil] ratios ($1/r_{bp}$ or $1/r_{bt}$) of 0, 50, 100, 200, 300, 400, and 500. The buffer conditions for the DNA titrations were 10 mM sodium cacodylate (pH 6.8), 300 mM NaCl, and 0.1 mM EDTA, while those for the RNA titrations were 10 mM sodium cacodylate (pH 6.9), 25 mM

[1] Abbreviations: poly(dT)·poly(dA)·poly(dT), poly(dA)·2poly(dT); poly(rU)·poly(rA)·poly(rU), poly(rA)·2poly(rU); bp, base pair(s); $r_{bp}$, [total berenil]/[base pairs]; bt, base triplet(s); $r_{bt}$, [total berenil]/[base triplets]; WC, Watson−Crick; HG, Hoogsteen; TSS, triplex to single strand; $T_m$, melting temperature; CD, circular dichroism; DSC, differential scanning calorimetry; NMR, nuclear magnetic resonance; UV, ultraviolet; EDTA, disodium salt of ethylenediaminetetraacetic acid; DAPI, 4′,6-diamidino-2-phenylindole.

NaCl, and 0.1 mM EDTA. Using this technique, the difference between the absorbance of a solution of berenil in the presence of nucleic acid and the absorbance of a solution of pure berenil at the same total concentration ($\Delta A$) is given by

$$\Delta A = C_B \Delta \epsilon l \quad (1)$$

where $C_B$ is the concentration of bound berenil, $l$ is the cell pathlength (1 cm in all the titration experiments), and $\Delta\epsilon$ is the difference between the extinction coefficients of bound and free berenil ($\epsilon_B - \epsilon_F$).

*Benesi–Hildebrand Analysis of the Isothermal Absorbance Titration Data To Derive Apparent Binding Affinities.* A *single mode* of berenil binding to a nucleic acid duplex or triplex can be described by the mass action equation

$$K_{app} = \frac{C_B}{C_F\left(\frac{C_N}{n} - C_B\right)} \quad (2)$$

where $C_F$ is the concentration of free berenil, $C_N$ is the total concentration of nucleic acid in base pairs or base triplets, $n$ is the apparent binding site size in base pairs or base triplets per bound berenil, and $K_{app}$ is the apparent binding constant. Under conditions where the nucleic acid is in large excess over berenil, one can assume that

$$\frac{C_N}{n} - C_B \approx \frac{C_N}{n} \quad (3)$$

At the $1/r_{bp}$ and $1/r_{bt}$ ratios of 50, 100, 200, 300, 400, and 500 used in the isothermal absorbance titrations described above, this assumption should be valid, even with apparent berenil binding site sizes of 11.5 and 12.7 for the DNA triplex and duplex structures, respectively (see Table 1 below). Given this assumption, eq 2 reduces to

$$K_{app} = \frac{C_B}{C_F(C_N/n)} \quad (4)$$

Substitution of eq 1 into eq 4 and rearranging yields

$$\frac{C_N C_T}{\Delta A} = \frac{C_N}{\Delta \epsilon l} + \frac{n}{K_{app} \Delta \epsilon l} \quad (5)$$

where $C_T$ is the total concentration of berenil. Equation 5, which is referred to as the Benesi–Hildebrand equation (Benesi & Hildebrand, 1949), predicts that a plot of $C_N C_T/\Delta A$ versus $C_N$ will be linear, with a slope of $1/\Delta\epsilon l$ and a $y$-intercept of $n/(K_{app}\Delta\epsilon l)$. If $n$ is known, then $K_{app}$ can be calculated from the slope divided by the $y$-intercept. We independently determined the value of $n$ from CD titrations, as described in the section that follows.

*CD Spectropolarimetry.* All CD experiments were performed on an AVIV model 60DS spectropolarimeter (AVIV Associates; Lakewood, NJ) which was equipped with a thermoelectrically controlled cell holder. The cell path length for all the CD studies was 1 cm. Isothermal nucleic acid titrations were performed at 25 °C by incrementally adding aliquots (1.5–50 $\mu$l) of concentrated nucleic acid polymer solutions (≈4 mM in base pair or base triplet) into solutions (2 mL) containing 18.5 $\mu$M berenil. After each addition, the CD spectra were recorded from either 270 or 280 nm to 450 nm, with an averaging time of 5 s. In these titrations, $1/r_{bp}$ and $1/r_{bt}$ ratios ranged from 0 to 32. The buffer conditions for the DNA titrations were 10 mM sodium cacodylate (pH 6.8), 300 mM NaCl, and 0.1 mM EDTA, while those for the RNA titrations were 10 mM sodium cacodylate (pH 6.9), 25 mM NaCl, and 0.1 mM EDTA. The final CD spectra were normalized to reflect equimolar berenil concentrations.

Ellipticity versus temperature profiles were measured at either 370 or 380 nm with a 10 s averaging time. The temperature was raised in 0.5 °C increments, and the samples were allowed to equilibrate for 1 min at each temperature setting. The DNA solutions were 300 $\mu$M in base triplet and contained 13.8 $\mu$M berenil, 10 mM sodium cacodylate (pH 6.8), 300 mM NaCl, and 0.1 mM EDTA. The RNA solutions were 200 $\mu$M in base triplet and contained 36.9 $\mu$M berenil, 10 mM sodium cacodylate (pH 6.9), 25 mM NaCl, and 0.1 mM EDTA.

*Viscometry.* Viscosity measurements were conducted using a Cannon-Manning size 75 capillary viscometer (Thomas Scientific, Swedesboro, NJ) submerged in a water bath maintained at 24.7 (±0.1) °C. Flow times were multiply measured to an accuracy of ±0.3 s, and the average time over all replicates was recorded. Viscosity studies on the poly(dA)·poly(dT) DNA duplex and the poly(dA)·2poly(dT) DNA triplex were conducted in a pH 6.8 buffer solution containing 10 mM sodium cacodylate, 300 mM NaCl, and 0.1 mM EDTA. Aliquots (3 $\mu$l) of 3.8 mM berenil were titrated into the viscometer containing polynucleotide solutions (1 mL) that were 500 $\mu$M in base pair or base triplet. Flow times in the range of 125–470 s were measured after each addition. Studies on the poly(rA)·poly(rU) RNA duplex and the poly(rA)·2poly(rU) RNA triplex were conducted in a pH 6.9 buffer solution containing 10 mM sodium cacodylate, 25 mM NaCl, and 0.1 mM EDTA. In these studies, aliquots (3 $\mu$l) of 7.1 mM berenil were titrated into the viscometer containing polynucleotide solutions (1 mL) that were 500 $\mu$M in base pair or base triplet. Flow times in the range of 125–230 s were measured after each addition.

*Isothermal Titration Calorimetry.* Isothermal calorimetric measurements were performed at 25 °C on a Microcal Omega titration calorimeter (Microcal, Inc., Amherst, MA). In a typical experiment, 5 $\mu$l aliquots of 2 mM berenil were injected from a 100 $\mu$l rotating syringe into an isothermal sample chamber containing 1.35 mL of a nucleic acid solution that was 400 $\mu$M in base pair or base triplet. The syringe was fitted with a stirrer blade at its end to ensure effective mixing of the sample (Wiseman et al., 1989). The duration of each injection was 8 s and the delay between injections was 5 min. Each injection generated a heat burst curve ($\mu$cal/s vs s). The area under each curve was determined by integration (using the Origin version 1.16 software; Microcal, Inc., Amherst, MA) to obtain a measure of the heat of berenil binding for that injection. The calorimeter was calibrated both electronically and chemically as previously described (Pilch et al., 1995). Experimental injections resulted in heats ranging from 5 to 65 $\mu$cal, depending on the host nucleic acid. The binding enthalpies ($\Delta H_B$) reported in this work reflect the total heat obtained by integration of the peaks resulting from the first two injections divided by the total concentration of injected berenil. These two injections resulted in $1/r_{bp}$ and $1/r_{bt}$ ratios of 29.1. At these ratios, most of the berenil should be bound

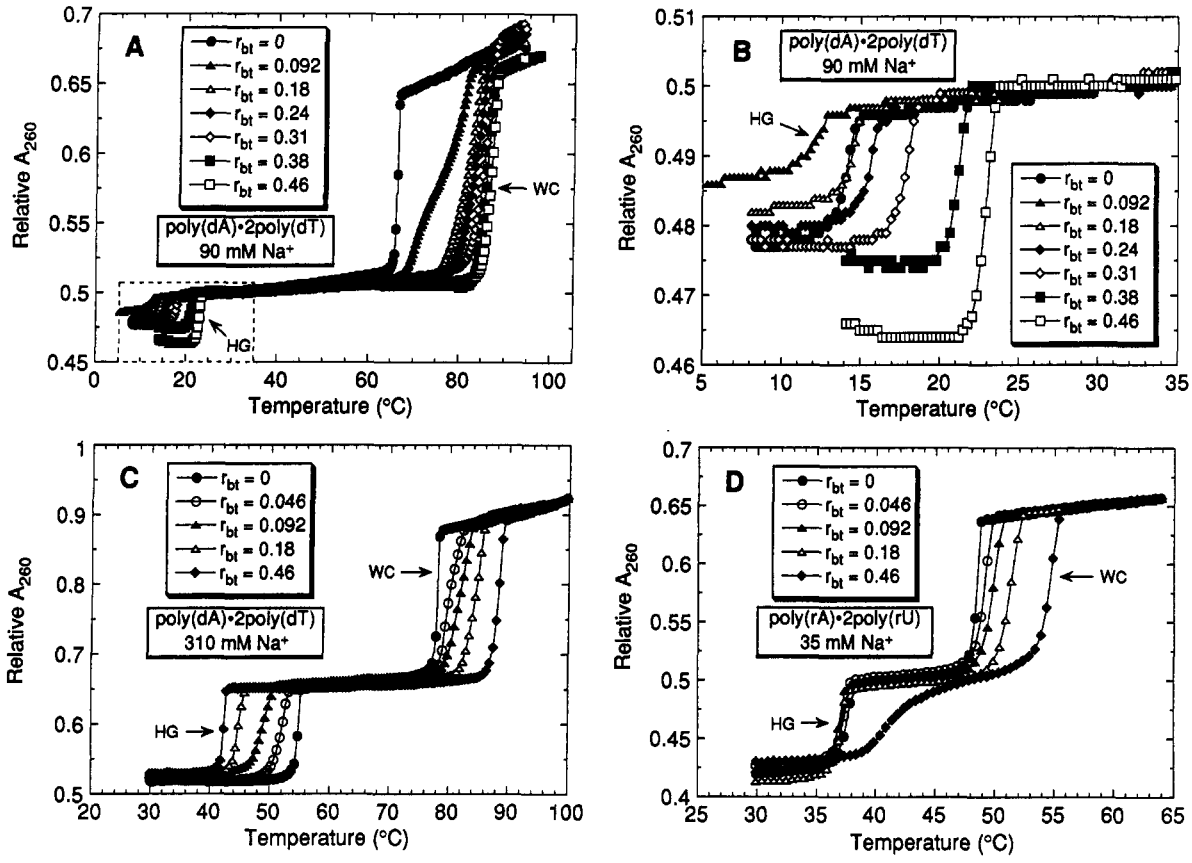


FIGURE 2: UV melting profiles at 260 nm and the indicated $Na^+$ concentrations for the poly(dA)•2poly(dT) DNA triplex (A-C) and the poly(rA)•2poly(rU) RNA triplex (D) and their berenil complexes at the indicated values of $r_{bt}$. Panel B presents an expanded view of the boxed region in panel A. For all the profiles, the Hoogsteen (HG) and Watson–Crick (WC) transitions are indicated. Studies on the poly(dA)•2poly(dT) triplex, were conducted at pH 6.8 in a buffer containing 10 mM sodium cacodylate, either 90 or 300 mM NaCl, and 0.1 mM EDTA. Studies on the poly(rA)•2poly(rU) triplex were conducted at pH 6.9 in a buffer containing 10 mM sodium cacodylate, 25 mM NaCl, and 0.1 mM EDTA. For clarity of presentation, the melting curves for a given triplex and its berenil complexes are normalized so as to produce similar absorbances at either the final temperature (for the DNA triplex in 310 mM $Na^+$ and the RNA triplex in 35 mM $Na^+$) or at 40 °C (for the DNA triplex in 90 mM $Na^+$).

considering the values of the binding constants that we have determined. Heat of dilution corrections were negligible since no detectable heat resulted from injection of 2 mM berenil into buffer or injection of buffer into a nucleic acid solution that was 400 $\mu$M in base pair or base triplet. Buffer conditions for experiments on the DNA solutions were 10 mM sodium cacodylate (pH 6.8), 300 mM NaCl, and 0.1 mM EDTA, while, for the RNA studies, the conditions were 10 mM sodium cacodylate (pH 6.9), 25 mM NaCl, and 0.1 mM EDTA.

*Differential Scanning Calorimetry (DSC).* Heat capacity ($\Delta C_p$) versus temperature ($T$) profiles for the thermally induced transitions of the free poly(dA)•2poly(dT) and poly(rA)•2poly(rU) triplexes and the free poly(dA)•poly(dT) and poly(rA)•poly(rU) duplexes, as well as their complexes with berenil, were measured using a Microcal MC-2 differential scanning calorimeter (Microcal, Inc., Amherst, MA). In all these experiments, the heating rate was 60 °C/h. Transition enthalpies ($\Delta H_{cal}$) were calculated from the areas under the heat capacity curves using the Origin version 1.16 software (Microcal, Inc., Amherst, MA). The DNA solutions were 300 $\mu$M in base pair or base triplet and contained 0, 70, or 91 $\mu$M berenil, 10 mM sodium cacodylate (pH 6.8), 300 mM NaCl, and 0.1 mM EDTA. The RNA solutions were 300 $\mu$M in base pair or base triplet and contained 0, 58, or 63 $\mu$M berenil, 10 mM sodium cacodylate (pH 6.9), 25 mM NaCl, and 0.1 mM EDTA.

## RESULTS AND DISCUSSION

*Berenil Binds to the Poly(dA)•2Poly(dT) DNA Triplex and either Enhances or Diminishes Its Thermal Stability in a Manner That Depends on Both the $Na^+$ Concentration and the Binding Density ($r_{bt}$).* Panels A and C of Figure 2 show the UV melting curves for the poly(dA)•2poly(dT) DNA triplex at 90 mM $Na^+$ (panel A) and 310 mM $Na^+$ (panel C) in the absence and presence of differing concentrations of berenil. Note that, at both $Na^+$ concentrations, the berenil-free triplex melts in two well-resolved sequential transitions. The lower temperature transition [the so-called Hoogsteen (HG) transition] reflects dissociation of the triplex to its component poly(dA)•poly(dT) duplex and poly(dT) single strand, while the higher temperature transition [the Watson–Crick (WC) transition] reflects denaturation of the remaining duplex into its component single strands (Riley et al., 1966; Pilch et al., 1990; Park & Breslauer, 1992). We find that, in the presence of either 90 or 310 mM $Na^+$, berenil binding thermally stabilizes the duplex to single strand equilibrium, with $\Delta T_m$ values of +20.8 °C in 90 mM $Na^+$ and +9.1 °C in 310 mM $Na^+$ at a $r_{bt}$ ratio of 0.46. This behavior is consistent with that which we and others previously have observed (Barceló & Portugal, 1993; Schmitz & Hübner, 1993; Pilch et al., 1995). However, inspection of the melting curves in panel C also reveals that in the presence of 310 mM $Na^+$ berenil binding thermally *destabilizes* the triplex

to duplex equilibrium, with a $\Delta T_m$ equal to −12.7 °C at a $r_{bt}$ ratio of 0.46. This observation is consistent with a model in which berenil binds more strongly to the duplex than to the triplex structure under these conditions, a behavior which we and others previously have observed for netropsin, a minor groove-binding ligand (Park & Breslauer, 1992; Durand et al., 1992). Interestingly, the reverse behavior has been observed for two intercalating ligands, ethidium bromide (Scaria & Shafer, 1991) and coralyne (Lee et al., 1993). The binding of these ligands to the poly(dA)·2poly(dT) DNA triplex thermally stabilizes the triplex to duplex equilibrium. However, as described in a later section, we find that berenil binding to the poly(dA)·2poly(dT) triplex exhibits viscometric properties characteristic of a nonintercalative mode of binding (e.g., minor groove binding). Consequently, it is tempting to conclude that minor groove binding ligands reduce the affinities of $(dT)_n$ third strands for their target $(dA)_n\cdot(dT)_n$ duplexes, while intercalating ligands enhance these affinities. However, as explained in the paragraph that follows, our studies at other salt concentrations (e.g., ≤125 mM $Na^+$) on the effects of berenil binding on the triplex to duplex equilibrium suggest that such a generalization is not always valid.

In contrast to the behavior just described for berenil binding at 310 mM $Na^+$, berenil binding in the presence of 90 mM $Na^+$ (Figure 2, panel B) thermally *stabilizes* the triplex to duplex equilibrium at $r_{bt}$ ratios ≥0.18 (e.g., at a $r_{bt}$ ratio of 0.46, $\Delta T_m$ equals +8.9 °C), while only thermally destabilizing this equilibrium at a $r_{bt}$ ratio of 0.092 ($\Delta T_m$ = −2.3 °C). These observations suggest that, in the presence of 90 mM $Na^+$, berenil binds more strongly to the duplex than to the triplex structure at a $r_{bt}$ ratio of 0.092, while binding more strongly to the triplex than to the duplex structure at $r_{bt}$ ratios ≥0.18. In fact, CD-detected berenil binding to the poly(dA)·2poly(dT) triplex (described in a later section) reveals two distinct binding events, which exhibit apparent binding site sizes ($n$) of 11.5 and 3.3 base triplets per berenil bound. Thus, at 90 mM $Na^+$, the $r_{bt}$ dependence we observe for the impact of berenil binding on the thermal stability of the triplex to duplex equilibrium is consistent with the relative berenil binding affinities for the duplex and triplex structures differing for the two binding events. Specifically, one can propose that the binding event which corresponds to $n$ = 11.5 exhibits a greater affinity for the duplex relative to the triplex structure, while the binding event with a $n$ value of 3.3 exhibits a greater affinity for the triplex relative to the duplex structure. The absence of such a $r_{bt}$ dependence when berenil binds to the poly(dA)·2poly(dT) triplex in the presence of 310 mM $Na^+$ suggests that, under these solution conditions, the relative berenil binding affinities for the duplex and triplex structures are similar for the two berenil binding events. It is gratifying to note that the [$Na^+$] dependence of the influence of berenil binding on the triplex to duplex equilibrium that we observe here is consistent with the behavior previously reported by Maurizot and co-workers (Durand et al., 1994) in studies on the interactions of berenil with an intramolecular DNA triplex containing 12 T·A·T base triplets.

On the basis of the foregoing presentation, it is clear that berenil binding properties are quite complex and highly dependent on solution conditions (e.g., temperature, salt), drug binding densities, and the structure of the host nucleic acid. To gain further insight into the DNA state targeted or induced by berenil binding, as well as to define the electrostatic contribution to the binding event, we have determined a complete temperature-, salt-, and berenil-dependent phase diagram for the poly(dA)·2poly(dT) triplex. These results are presented in the Appendix to this paper. This appended material is designed to underscore the importance of such multiparametric characterizations for establishing meaningful comparisons of ligand binding properties over a range of solution conditions.

*Berenil also Binds to the Poly(rA)·2Poly(rU) RNA Triplex and either Enhances or Diminishes Its Thermal Stability Depending on the Drug Binding Density.* Panel D of Figure 2 presents the UV melting curves for the poly(rA)·2poly(rU) RNA triplex in the absence and presence of differing concentrations of berenil. Note that, as with the DNA host triplex, the berenil-free RNA triplex melts in two well-resolved sequential transitions. The lower temperature HG transition reflects dissociation of the RNA triplex to the poly(rA)·poly(rU) duplex and the poly(rU) single strand, while the higher temperature WC transition reflects denaturation of the remaining duplex into its component single strands (Krakauer & Sturtevant, 1968). As with the DNA duplex, the thermal stability of the RNA duplex increases as $r_{bt}$ increases from 0 to 0.46 (with a $r_{bt}$ ratio of 0.46 corresponding to a $\Delta T_m$ of +6.2 °C). This influence of drug binding on the duplex to single strand transition is consistent with what we previously have observed (Pilch et al., 1995). Inspection of panel D also reveals that berenil binding weakly decreases the thermal stability of the RNA triplex at $r_{bt}$ ratios ≤ 0.18 (e.g., a $r_{bt}$ ratio of 0.092 corresponds to a $\Delta T_m$ of −0.6 °C), while exerting a thermally stabilizing influence on the triplex at a $r_{bt}$ ratio of 0.46 ($\Delta T_m$ = +3.5 °C). These observations suggest that berenil binds more strongly to the duplex than to the triplex structure at $r_{bt}$ ratios ≤ 0.18, while binding more strongly to the triplex than to the duplex structure at a $r_{bt}$ ratio of 0.46. As described in a later section, CD-detected berenil binding to the poly(rA)·2poly(rU) RNA triplex reveals two distinct binding events, with $n$ values of 4.8 and 1.2 base triplets per berenil bound. Thus, as with the DNA host, the $r_{bt}$ dependence we observe for the effect of berenil binding on the thermal stability of the RNA triplex is consistent with the relative berenil binding affinities for the duplex and triplex states differing for the two berenil binding events. Specifically, one can propose that the binding event with a site size of 4.8 exhibits a greater affinity for the duplex relative to the triplex, while the binding event with a site size of 1.2 exhibits a greater affinity for the triplex relative to the duplex state. To the best of our knowledge, our observation of berenil-induced changes in the thermal stability of the poly(rA)·2poly(rU) triplex provides the first demonstration of a ligand other than ethidium bromide binding to a RNA triplex.

Inspection of Figure 2 reveals that a lower ionic strength (35 mM $Na^+$) is required to observe berenil-induced changes in the thermal stability of the RNA triplex relative to the DNA triplex (90 or 310 mM $Na^+$). This observation suggests that nonelectrostatic interactions contribute more when dicationic berenil binds to the DNA host triplex than when it binds to the RNA host triplex. Such a conclusion is consistent with results described in a later section, which demonstrate that berenil binds to the DNA triplex more strongly than to the RNA triplex.

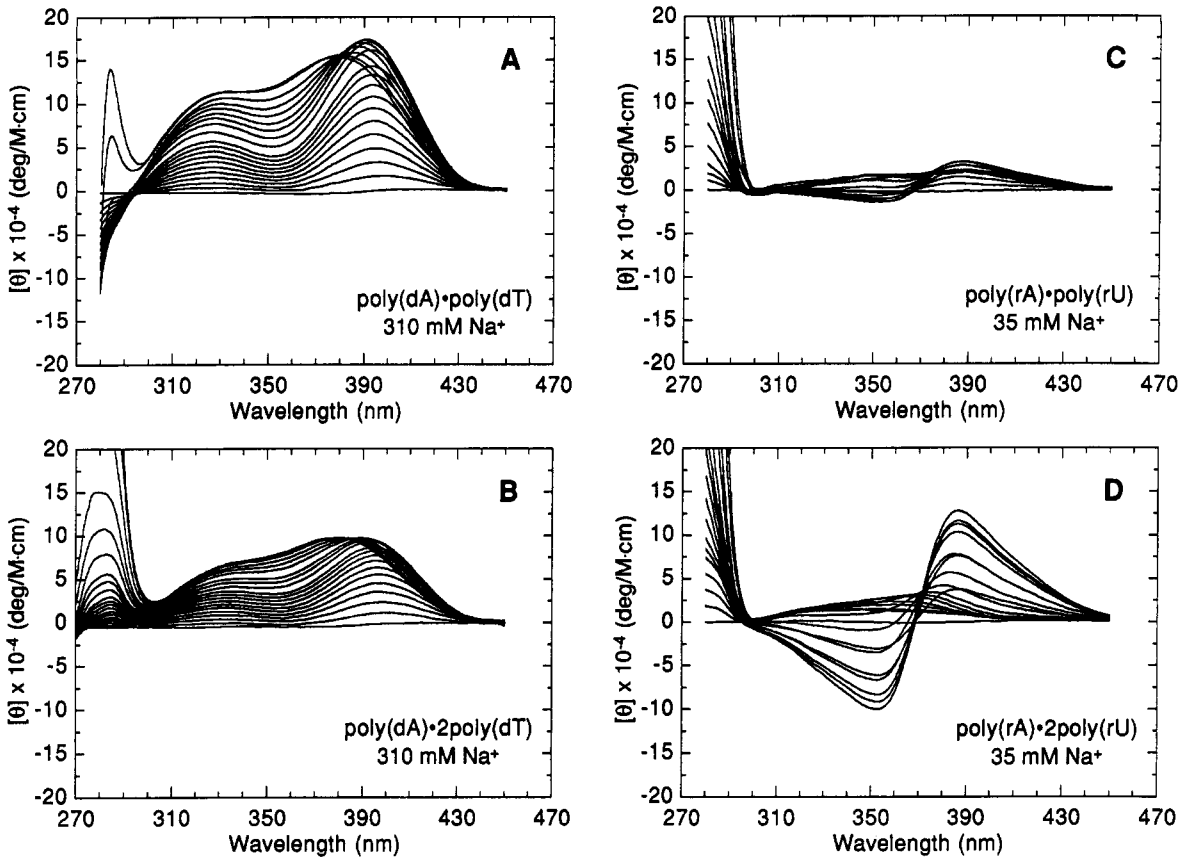


FIGURE 3: CD titrations at 25 °C of berenil (18.5 $\mu$M) with poly(dA)•poly(dT) (A); poly(dA)•2poly(dT) (B); poly(rA)•poly(rU) (C); and poly(rA)•2poly(rU) (D). From bottom to top, at either 330 nm (for the DNA titrations) or 420 nm (for the RNA titrations), the CD spectra correspond to $1/r_{bp}$ or $1/r_{bt}$ ratios ranging from 0 to 23−32. The DNA titrations were conducted at pH 6.8 in a buffer containing 10 mM sodium cacodylate, 300 mM NaCl, and 0.1 mM EDTA, while the RNA titrations were conducted at pH 6.9 in a buffer containing 10 mM sodium cacodylate, 25 mM NaCl, and 0.1 mM EDTA. Molar ellipticities, [$\theta$], are in units of deg/M•cm, where M refers to moles of total berenil per liter.

As with the DNA host, to gain further insight into the RNA state targeted or induced by berenil binding, as well as to define the electrostatic contribution to the binding event, we also have determined a complete temperature-, salt-, and berenil-dependent phase diagram for the poly(rA)•2poly(rU) triplex. These results are presented in the Appendix to this paper. As previously noted, such phase diagrams are important when defining and comparing the nucleic acid binding properties of a ligand over a range of solution conditions.

The results presented above describe our use of UV melting curves to define the influence of berenil binding on the temperature-dependent transitions of a DNA and a RNA triplex. In the sections that follow, we describe how circular dichroism (CD) measurements can be used to characterize further the triplex-binding properties of berenil.

*CD-Detected Berenil Binding to the DNA Triplex Reveals Two Apparent Binding Site Sizes.* In addition to the UV thermal denaturation studies described above, CD spectropolarimetry provides a second means for detecting and characterizing ligand binding. Panels A and B of Figure 3 show the CD spectra from 270 or 280 nm to 450 nm obtained by incremental titration of either poly(dA)•poly(dT) (panel A) or poly(dA)•2poly(dT) (panel B) into a solution of berenil. Neither free berenil nor any of the drug-free DNA structures (spectra not shown) exhibit CD signals between 300 and 450 nm. However, upon addition of either duplex or triplex DNA to a berenil solution, substantial CD signals arise in this wavelength range. These induced CD signals are indicative of interactions between berenil and each of the target DNA structures and can be used to detect and to monitor the *CD-active* mode of berenil binding.

Inspection of panels A and B of Figure 3 reveals the absence of a single discrete isoelliptic point for either DNA host structure. In fact, for the poly(dA)•poly(dT) duplex, two isoelliptic points are observed at 295 and 380 nm, while, for the poly(dA)•2poly(dT) triplex, two isoelliptic points occur at 275 and 386 nm. The isoelliptic points which occur at either 275 or 295 nm are shared by the spectra which correspond to free berenil and by those which correspond to the drug-bound complexes with $1/r_{bp}$ or $1/r_{bt}$ values $\leq 6$. By contrast, the isoelliptic points which occur at either 380 or 386 nm are shared by the drug-bound spectra which correspond to $1/r_{bp}$ or $1/r_{bt}$ values $>6$. *The absence of a single distinct isoelliptic point for both the duplex and the triplex is consistent with more than one optically detectable event when either poly(dA)•poly(dT) or poly(dA)•2poly(dT) serves as the host DNA structure.* This observation may reflect more than one mode of berenil binding. Alternatively, it may reflect a binding-induced conformational change in the host DNA structure. Either or both of these possibilities could give rise to the observed lack of a single discrete isoelliptic point.

Single-wavelength titration curves extracted from the CD spectra shown in panels A and B of Figure 3 are presented in panels A and B of Figure 4. In these curves, the points

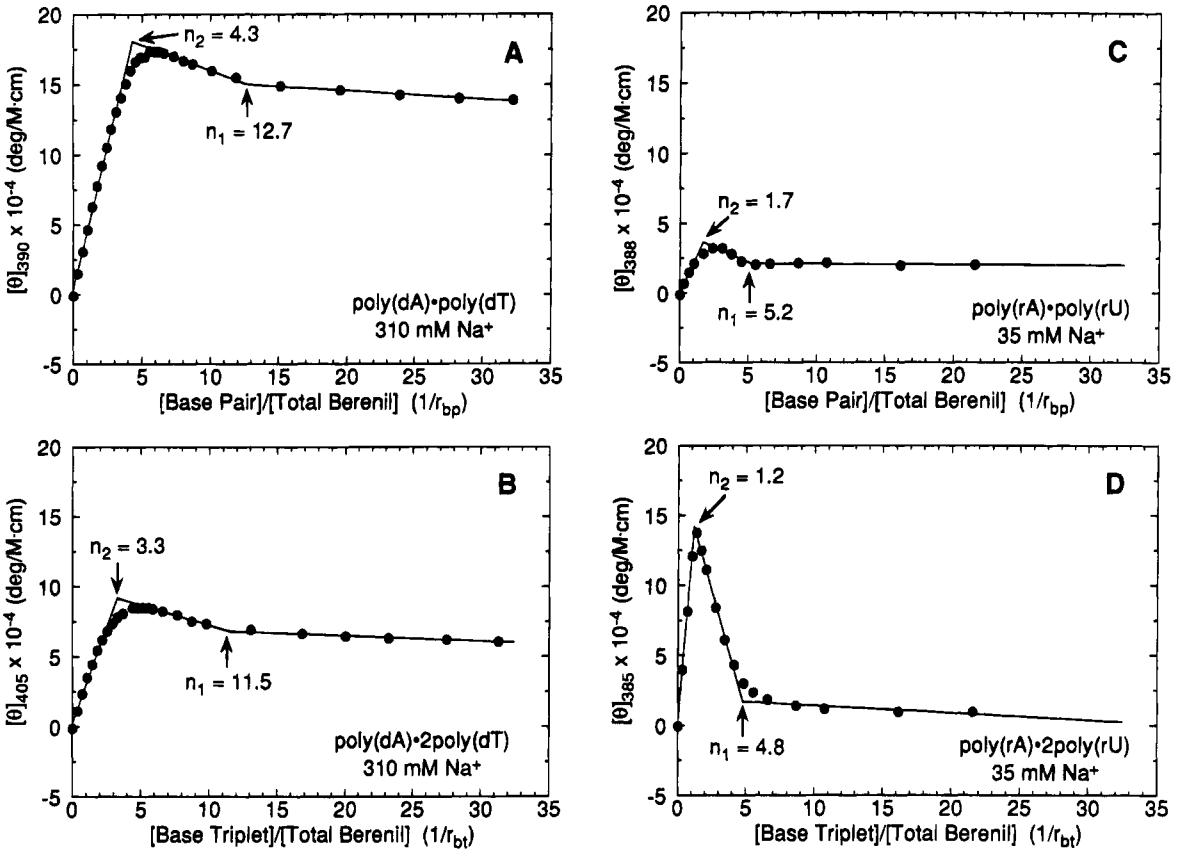


FIGURE 4: Normalized molar (moles of total berenil/liter) ellipticities at the indicated wavelengths versus $1/r_{bp}$ or $1/r_{bt}$ for the titrations at 25 °C of berenil with poly(dA)•poly(dT) (A); poly(dA)•2poly(dT) (B); poly(rA)•poly(rU) (C); and poly(rA)•2poly(rU) (D). The solid lines reflect linear least-squares fits of each apparent linear domain of the experimental data (●) before and after the apparent inflection points. The apparent binding site sizes ($n$) in units of base pairs or base triplets per berenil bound are indicated and correspond to the apparent inflection points. Solution conditions are the same as those described in the legend of Figure 3.

represent the experimental molar ellipticities of the drug, while the solid lines reflect linear least-squares fits of each apparent linear domain before and after the apparent inflection points. Note that two inflection points are observed for berenil binding to both DNA host structures. The presence of two inflection points is consistent with several possible binding models. In one model, the drug binds by a "singular" motif with an apparent site size defined by one inflection point, while the second inflection point reflects a binding-induced conformational change in the host DNA structure. A second model consistent with two inflection points involves the drug binding by two different motifs, each with different binding site sizes. Our data do not permit us to differentiate between these two possible interpretations or a hybrid interpretation involving both models. Instead, we simply note that the $1/r_{bp}$ or $1/r_{bt}$ values which correspond to the two inflection points provide lower estimates for the apparent number of base pairs or base triplets influenced by each event. These values must be considered lower estimates because $1/r_{bp}$ and $1/r_{bt}$ reflect the ratios of [base pairs] or [base triplets] to [total berenil] rather than to [bound berenil]. For the host DNA and RNA structures used in this study, these values are summarized in Table 1. Note that when either the poly(dA)•poly(dT) DNA duplex or the poly(dA)•2poly(dT) DNA triplex serves as the host structure, one event influences an apparent site size of either 12.7 or 11.5 base pairs or base triplets per berenil bound, respectively, while the other is associated with an apparent site size of either 4.3 or 3.3 base pairs or base triplets per berenil bound, respectively. We believe that the smaller size reflects a specific mode of berenil binding to a specific DNA site since it is in agreement with DNase footprinting (Portugal & Waring, 1986, 1987), crystallographic (Brown et al., 1990, 1992), and NMR (Yoshida et al., 1990; Shafer et al., 1990; Lane et al., 1991; Jenkins et al., 1993) studies of berenil complexation with duplex DNA. On the basis of this agreement, it is tempting to ascribe this site size to the minor groove binding motif observed in structural studies of

Table 1: Apparent Binding Site Sizes Associated with Berenil Interacting with the Poly(dA)•2Poly(dT) and Poly(rA)•2Poly(rU) Triplexes and with the Corresponding Poly(dA)•Poly(dT) and Poly(rA)•Poly(rU) Duplexes[a]

| | | apparent binding site size[b] (bp or bt/berenil bound) | |
|---|---|---|---|
| host nucleic acid | [$Na^+$] (mM) | $n_1$ | $n_2$ |
| poly(dA)•poly(dT) | 310 | 12.7 ± 1.3 | 4.3 ± 0.4 |
| poly(dA)•2poly(dT) | 310 | 11.5 ± 1.3 | 3.3 ± 0.3 |
| poly(rA)•poly(rU) | 35 | 5.2 ± 0.6 | 1.7 ± 0.2 |
| poly(rA)•2poly(rU) | 35 | 4.8 ± 0.4 | 1.2 ± 0.1 |

[a] Solution conditions for all polydeoxyribonucleotide experiments were 10 mM sodium cacodylate (pH 6.8), 300 mM NaCl, and 0.1 mM EDTA, while those for all polyribonucleotide experiments were 10 mM sodium cacodylate (pH 6.9), 25 mM NaCl, and 0.1 mM EDTA. All experiments were carried out at 25 °C. [b] Apparent binding site sizes were determined from the single wavelength, induced CD titration curves ([$\theta$] vs $1/r_{bp}$ or $1/r_{bt}$) shown in Figure 4. These apparent binding site sizes should be considered lower limits since $1/r_{bp}$ and $1/r_{bt}$ reflect the ratios of [base pairs] or [base triplets] to [total berenil] rather than to [bound berenil]. Errors reflect the 95% confidence limits from linear regression analyses of each apparent linear domain before and after the apparent inflection points.

berenil–DNA complexes. Furthermore, our viscometric results, described in a later section, are consistent with nonintercalative binding. The events associated with the larger apparent site sizes may reflect allosteric conformational changes in the host DNA structures induced by berenil binding, rather than a specific mode of binding. This type of allosteric behavior previously has been observed by Nordén and co-workers (Eriksson et al., 1993) in CD studies of DAPI (4′,6-diamidino-2-phenylindole) binding to the poly[d(A-T)]$_2$ duplex, as well as by us and others in studies of ethidium, propidium, and/or daunomycin binding to the poly(dA)·poly(dT) duplex (Wilson et al., 1985; Breslauer et al., 1987; Herrera & Chaires, 1989; Scaria & Shafer, 1991) and the poly(dA)·2poly(dT) triplex (Scaria & Shafer, 1991).

*Berenil Exhibits a Higher Saturation Binding Density for the DNA Triplex Than for the Corresponding DNA Duplex.* Inspection of the data listed in Table 1 reveals that one of the apparent binding site sizes for the poly(dA)·2poly(dT) triplex (3.3 base triplets per berenil bound) is smaller than the corresponding site size for the poly(dA)·poly(dT) duplex (4.3 base pairs per berenil bound). Thus, at saturation, the poly(dA)·2poly(dT) triplex binds *more* berenil molecules than the poly(dA)·poly(dT) duplex. As described in a later section, berenil binding to both these DNA structures exhibits viscometric properties characteristic of nonintercalative (e.g., minor groove) binding. These collective observations suggest that occupancy of the major groove by a third strand can affect the drug binding capacity of the minor groove. We (Park & Breslauer, 1992) previously have observed this type of groove "cross-talk" in a study probing the interactions of the minor groove-binding ligand netropsin with the poly(dA)·2poly(dT) triplex. However, in contrast to our results with netropsin, we find here that, at saturation, the poly(dA)·2poly(dT) triplex binds *more* berenil molecules than the corresponding poly(dA)·poly(dT) duplex. Thus, the nature and magnitude of differential duplex versus triplex drug binding capacities (groove "cross-talk") may depend on more than just the general mode of binding, with influences being exerted by the specific drug structure and/or subtle differences within a common binding motif.

*CD-Detected Berenil Binding to the RNA Triplex also Reveals Two Apparent Binding Site Sizes.* Panels C and D of Figure 3 show the CD spectra from 280 to 450 nm obtained by titration of either the poly(rA)·poly(rU) RNA duplex (panel C) or the poly(rA)·2poly(rU) RNA triplex (panel D) into a solution of berenil at 35 mM $Na^+$. As observed for the DNA structures, addition of either the RNA duplex or triplex into a berenil solution induces a CD signal between 300 and 450 nm, consistent with berenil also binding to these host structures. Note that, at $1/r_{bp}$ or $1/r_{bt}$ ratios less than 5, berenil exhibits a substantially larger induced CD signal when bound to the RNA triplex than when bound to the RNA duplex, an observation consistent with berenil adopting different structural/electronic properties when bound to these two RNA structures at high binding densities. Further, note that the families of CD spectra obtained from these titrations do not exhibit single isoelliptic points. The absence of an isoelliptic point is consistent with *more than one optically detected event when either poly(rA)·poly(rU) or poly(rA)·2poly(rU) serves as the host structure.* The same potential explanations can be offered for this observation as were presented above for berenil binding to the DNA host structures.

Panels C and D of Figure 4 show the single-wavelength titration curves derived from the corresponding families of CD spectra shown in panels C and D of Figure 3. The two inflection points observed in these titration curves (at either 5.2 and 1.7 base pairs per berenil bound or 4.8 and 1.2 base triplets per berenil bound) are consistent with one of the several binding models described above for the DNA host structures. As with the DNA hosts, we propose that the apparent binding site sizes of 5.2 and 4.8 are associated with the primary mode of berenil binding. However, one should not assume that this mode exclusively is minor groove binding for all host structures since our viscometric measurements (described below) reveal that berenil binding to the poly(rA)·poly(rU) duplex, in fact, exhibits properties characteristic of intercalation. The smaller binding site sizes we observe (1.7 and 1.2) may correspond to a secondary mode of berenil binding in which electrostatically driven stacking of the drug on the helix exterior occurs under conditions of high drug loading (low $1/r_{bp}$ or $1/r_{bt}$ ratios). Such a secondary binding mode would be enhanced under conditions of low ionic strength, as are used in the RNA titrations (35 mM $Na^+$), and would result in very few base pairs or base triplets being covered per bound drug molecule. This secondary binding motif is common among, but need not be restricted to, intercalating ligands (Neidle & Abraham, 1984). In comparing the berenil binding properties of the DNA and RNA hosts, one should resist the temptation to define the mode of binding based exclusively on the binding site sizes or the order in which they occur, both of which differ for the two families of host structures.

*Relative Berenil Binding Affinities for the Duplex and Triplex Structures Determined by Benesi–Hildebrand Analyses of Isothermal Absorbance Binding Data.* Panel A of Figure 5 shows Benesi–Hildebrand plots for berenil binding to the poly(dA)·poly(dT) DNA duplex and the poly(dA)·2poly(dT) DNA triplex, while panel B of Figure 5 shows the corresponding plots for berenil binding to the poly(rA)·poly(rU) RNA duplex and the poly(rA)·2poly(rU) RNA triplex. Recall that the Benesi–Hildebrand equation (eq 5) is predicated on an assumed single mode of binding, a reasonable assumption over the range of $1/r_{bp}$ or $1/r_{bt}$ ratios (50–500) used in our isothermal absorbance experiments. Note that, as predicted by the Benesi–Hildebrand equation, all four plots are linear, supporting both the validity of the assumptions inherent in this equation and the use of this equation to analyze the absorbance data (see Materials and Methods). The binding parameters derived from the slopes and $y$-intercepts of these plots according to eq 5 are summarized in Table 2.

Recall that our CD titrations (Figures 3 and 4) are consistent with more than one binding event when berenil binds to the nucleic acid structures studied here. However, such CD data do not allow us to resolve unambiguously the molar ellipticities corresponding to the different bound forms of berenil. The absence of such information precludes us from constructing Scatchard plots that could be used to obtain meaningful binding constants via McGhee–von Hippel analyses (McGhee & von Hippel, 1974). Alternatively, we have used a Benesi–Hildebrand analysis of isothermal absorbance titrations to obtain a quantitative estimate of the apparent berenil binding affinities at low drug binding densities (i.e., high $1/r_{bp}$ or $1/r_{bt}$ ratios). Since such an analysis does not explicitly account for the overlapping

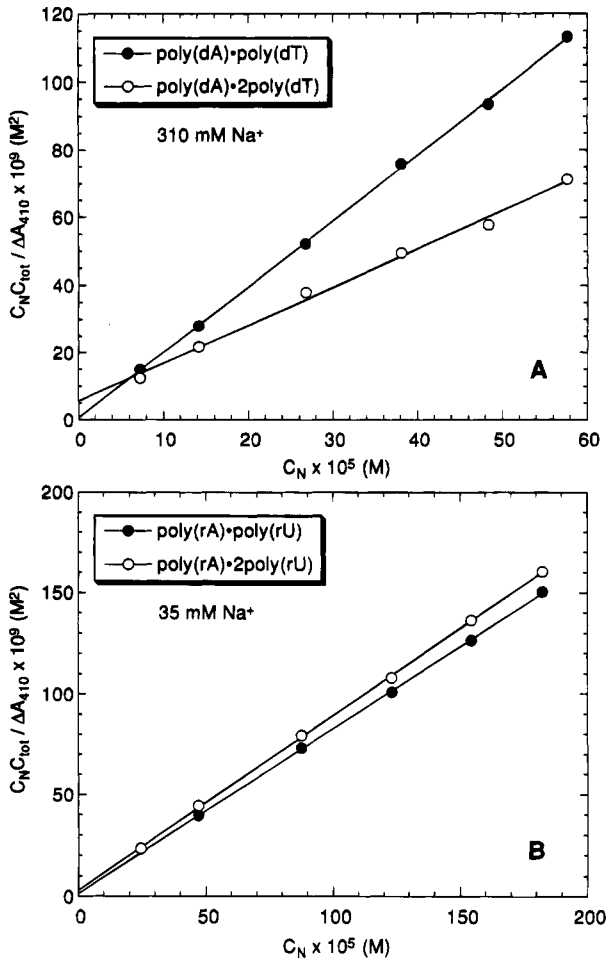


FIGURE 5: (A) Benesi–Hildebrand plots for the absorbance titrations at 25 °C of berenil with poly(dA)•poly(dT) (●) and poly(dA)•2poly(dT) (○). (B) Benesi–Hildebrand plots for the absorbance titrations at 25 °C of berenil with poly(rA)•poly(rU) (●) and poly(rA)•2poly(rU) (○). The solid lines reflect linear least-squares fits of the experimental data. The experimental data points reflect $1/r_{bp}$ or $1/r_{bt}$ ratios of 50, 100, 200, 300, 400, and 500. Solution conditions are the same as those described in the legend of Figure 3.

binding sites that may exist on a nucleic acid polymer lattice, the apparent berenil binding affinities so obtained should be considered as approximations.

*Berenil Binding to Triplex Versus Duplex Structures.* Inspection of the data listed in Table 2 reveals a greater $\Delta\epsilon_{410}$ for berenil binding to the poly(dA)•2poly(dT) triplex (8860) than for berenil binding to the poly(dA)•poly(dT) duplex (5150). In other words, relative to free berenil, the absorbance spectrum of triplex-bound berenil is substantially more red-shifted than is the absorbance spectrum of duplex-bound berenil. It is likely that this difference in $\Delta\epsilon_{410}$ reflects structural distinctions between the berenil–triplex and berenil–duplex complexes, which, in turn, may, in part, derive from conformational differences between the initial drug-free DNA duplex and triplex states. In fact, conformational differences between the DNA duplex and triplex states have been observed by Arnott and co-workers (Arnott & Selsing, 1974; Arnott et al., 1976). Their fiber diffraction studies reveal that the poly(dA)•poly(dT) duplex adopts a non-canonical B-like conformation, while the poly(dA)•2poly(dT) triplex adopts a more A-like conformation.

Further inspection of the data in Table 2 reveals that, unlike the differential $\Delta\epsilon_{410}$ values for the DNA structures, the $\Delta\epsilon_{410}$ values for berenil binding to both the poly(rA)•poly(rU) RNA duplex and the poly(rA)•2poly(rU) RNA triplex are similar (12 300 and 11 600, respectively). Furthermore, these $\Delta\epsilon_{410}$ values are significantly greater than those for either of the DNA structures. In this connection, Arnott et al. (1973, 1976) have shown that the poly(rA)•poly(rU) RNA duplex and the poly(rA)•2poly(rU) RNA triplex both adopt A-like conformations. This similarity in the global conformations of the initial drug-free states may, in part, account for the similarity in $\Delta\epsilon_{410}$ for berenil binding to both RNA structures. With regard to the differences in the magnitudes of the $\Delta\epsilon_{410}$ values we measure for berenil binding to the DNA and RNA host structures, it may be that berenil binding to A-like nucleic acid structures yields a larger red-shift in the drug absorbance spectrum than berenil binding to B-like nucleic acid structures. Clearly, further studies are required to assess the generality of this observation.

To derive binding constants at 25 °C ($K_{app}^{25°C}$) from the slope and $y$-intercept values of the Benesi–Hildebrand plots, it is necessary to select an appropriate apparent binding site size ($n_{app}$). To make this selection, we assumed that berenil interacts with its nucleic acid targets only by that mode of binding which corresponds to the larger of the two site sizes listed in Table 1 (the $n_1$ values). This assumption is reasonable considering the linearity of the Benesi–Hildebrand plots and the large $1/r_{bp}$ and $1/r_{bt}$ ratios (50–500) used in the absorbance titrations. Thus, the appropriate CD-derived $n_1$ values were used in the derivation of the $K_{app}^{25°C}$ values summarized in Table 2.

Inspection of the data in Table 2 reveals that, in the presence of 310 mM $Na^+$, berenil binds the poly(dA)•poly(dT) DNA duplex with an 18-fold higher affinity than the poly(dA)•2poly(dT) DNA triplex ($4.3 \times 10^6$ versus $2.4 \times 10^5$ $M^{-1}$). This observation is consistent with the significant berenil-induced reduction in the thermal stability of the triplex to duplex equilibrium observed in panel C of Figure 2. As described in a later section, berenil binding to both of these DNA structures exhibits viscometric properties characteristic of nonintercalative (e.g., minor groove) binding. These collective observations suggest that occupancy of the major groove by a third strand can affect the affinity of a ligand for the minor groove. This type of DNA groove cross-talk may originate from conformational changes in the duplex (i.e., the WC-paired strands) induced by the presence of the third strand in the major groove, a possibility consistent with the fiber diffraction findings of Arnott and co-workers (Arnott & Selsing, 1974).

Further inspection of the data in Table 2 reveals that, in the presence of 35 mM $Na^+$, berenil binds the poly(rA)•poly(rU) RNA duplex with only a 2.4-fold higher affinity than the poly(rA)•2poly(rU) RNA triplex ($3.4 \times 10^5$ versus $1.4 \times 10^5$ $M^{-1}$). This observation is consistent with the small degree of berenil-induced reduction in the thermal stability of the triplex to duplex equilibrium observed in panel D of Figure 2. As described in a later section, berenil binding to the poly(rA)•poly(rU) RNA duplex exhibits viscometric properties characteristic of intercalation, while berenil binding to the poly(rA)•2poly(rU) RNA triplex exhibits viscometric properties characteristic of nonintercalative (e.g., minor groove) binding. Thus, berenil intercalation into the poly(rA)•poly(rU) RNA duplex appears to be associated with a

Table 2: Binding Parameters for the Complexation of Berenil with the Poly(dA)·2Poly(dT) and Poly(rA)·2Poly(rU) Triplexes and with the Corresponding Poly(dA)·Poly(dT) and Poly(rA)·Poly(rU) Duplexes[a]

| host nucleic acid | $[Na^+]$ (mM) | $n_{app}$ [b] (bp or bt/ligand) | $\Delta\epsilon_{410}$ [c] ($M^{-1}cm^{-1}$) | $K_{app}^{25°C}/n_{app}$ ($M^{-1}$) | [c] $K_{app}^{25°C}$ ($M^{-1}$) |
|---|---|---|---|---|---|
| DNA | | | | | |
| poly(dA)·poly(dT) | 310 | 12.7 | 5150 | $3.4 \times 10^5$ | $4.3 \times 10^6$ |
| poly(dA)·2poly(dT) | 310 | 11.5 | 8860 | $2.1 \times 10^4$ | $2.4 \times 10^5$ |
| RNA | | | | | |
| poly(rA)·poly(rU) | 35 | 5.2 | 12 300 | $6.5 \times 10^4$ | $3.4 \times 10^5$ |
| poly(rA)·2poly(rU) | 35 | 4.8 | 11 600 | $2.9 \times 10^4$ | $1.4 \times 10^5$ |

[a] Binding parameters were determined according to eq 5 from the slopes and $y$-intercepts of the Benesi–Hildebrand plots in Figure 5. Experimental conditions are as stated in the footnote of Table 1. [b] The apparent binding site sizes ($n_{app}$) correspond to the $n_1$ values listed for each nucleic acid structure in Table 1. [c] $K_{app}^{25°C}$ denotes the apparent berenil binding affinity at 25 °C, while $\Delta\epsilon_{410}$ denotes the difference in the extinction coefficient at 410 nm between nucleic acid-bound and free berenil ($\epsilon_{410,bound} - \epsilon_{410,free}$).

slightly higher affinity than berenil nonintercalative binding to the poly(rA)·2poly(rU) RNA triplex.

As an aside, one should note that the $K_{app}^{25°C}$ we determine here ($3.4 \times 10^5$ $M^{-1}$) for the binding of berenil to the poly(rA)·poly(rU) RNA duplex in 35 mM $Na^+$ is roughly 4-fold lower than that ($1.4 \times 10^6$ $M^{-1}$) we derived previously (Pilch et al., 1995) using a "$\Delta T_m$ method" (Crothers, 1971). This discrepancy may reflect contributions from a secondary mode of binding in our previous study. In the $\Delta T_m$ method, $K_{app}^{25°C}$ values are determined from the difference between the thermal stability of the berenil-free RNA duplex and the thermal stability of this duplex when saturated with berenil that is bound only by the primary mode, namely, that binding mode which corresponds to a site size of 5.2 (i.e., at a $1/r_{bp}$ ratio of 5.2). However, at a $1/r_{bp}$ ratio of 5.2, a small amount of berenil binding via a secondary mode which corresponds to a site size of 1.7 also may occur (see Table 1). In fact, as described in a later section, the WC transition from the DSC profile of a berenil–poly(rA)·2poly(rU) complex at a $1/r_{bt}$ ratio of 4.8 exhibits properties consistent with a small amount of secondary binding. This "contaminating" contribution from secondary binding would make $\Delta T_m$ values erroneously high, since both the primary and secondary modes of berenil binding act to enhance the thermal stability of the duplex. In such a case, the binding constant calculated using the $\Delta T_m$ method would be higher than that calculated by the isothermal Benesi–Hildebrand method, which, by virtue of its requirement for large $1/r_{bp}$ ratios, does not suffer from possible "contaminations" due to secondary modes of binding.

*Berenil Binding to DNA versus RNA Triplex Structures.* The thermal instability of the poly(dA)·2poly(dT) DNA triplex at $Na^+$ concentrations ≤110 mM, coupled with the low degree of berenil binding to the poly(rA)·2poly(rU) RNA triplex at $Na^+$ concentrations ≥110 mM, precluded us from defining identical ionic conditions under which berenil binding to both triplexes could be studied and compared. Nevertheless, the data in Table 2 reveal that berenil exhibits a slightly greater apparent binding affinity for the poly(dA)·2poly(dT) DNA triplex at 310 mM $Na^+$ relative to the poly(rA)·2poly(rU) RNA triplex at 35 mM $Na^+$ ($2.4 \times 10^5$ versus $1.4 \times 10^5$ $M^{-1}$). Despite the differing $Na^+$ concentrations, this observation suggests that berenil binds the DNA triplex with a greater apparent affinity than the RNA triplex, since changes in nucleic acid binding affinities of positively charged drugs generally are inversely proportional to changes in $Na^+$ concentration. In the aggregate, the data in Table 2 allow us to define the following hierarchy for berenil binding affinity: poly(dA)·poly(dT) > poly(dA)·2poly(dT) > poly(rA)·poly(rU) ≈ poly(rA)·2poly(rU). Conformational differences between B-like and A-like nucleic acid structures (particularly the topologies of the grooves) may contribute to these differences in apparent binding affinities. As discussed above, the rank order of the DNA duplex and triplex within this hierarchy can be reversed at $Na^+$ concentrations ≤125 mM and $1/r_{bt}$ ratios ≥0.18. Note that the apparent binding constants ($K_{app}^{25°C}$) listed in the final column of Table 2 are dependent on the apparent binding site sizes ($n_{app}$), which differ for the DNA and RNA host structures (see column 3 in Table 2). However, the same hierarchy of berenil binding affinity that emerges from the values of $K_{app}^{25°C}$ also is observed in the values of $K_{app}^{25°C}/n_{app}$ (column 5, Table 2), which reflect the the apparent binding constants prior to scaling for site size.

In the next section, we describe the use of viscometric techniques to characterize further the nature of the modes by which berenil binds to the DNA and RNA triplex structures studied here.

*Viscometric Measurements Suggest That Berenil Binds both the DNA and the RNA Triplexes by an Apparent Nonintercalative Mode.* The primary mode of binding by which a ligand interacts with a polymeric host nucleic acid structure can be investigated by viscometric techniques (Bloomfield et al., 1974, and references therein). If one treats a DNA or RNA helix as a rod-like molecule and assumes negligible changes in the axial ratio upon ligand binding (Cohen & Eisenberg, 1969), the relationship between the relative solution viscosity ($\eta/\eta_o$) and the relative contour length ($L/L_o$) is given by the expression (Müller & Crothers, 1968; Bloomfield et al., 1974)

$$\frac{L}{L_o} = \sqrt[3]{\frac{\eta}{\eta_o}} \qquad (6)$$

where $L_o$ and $\eta_o$ denote the apparent molecular length and solution viscosity in the absence of ligand. Based on this equation, an increase in relative viscosity generally reflects an increase in apparent molecular length. Ligand insertion between stacked bases within a linear host helix (intercalation) is associated with a lengthening of the nucleic acid. Thus, a ligand-induced increase in the viscosity of a nucleic acid solution is consistent with (but does not prove) an intercalative mode of binding. Conversely, the lack of a ligand-induced increase in the viscosity of a nucleic acid solution is consistent with (but does not prove) a nonintercalative mode of binding, such as minor groove binding.

Figure 6 shows the effect of berenil binding on the apparent molecular lengths of the two host triplexes and two

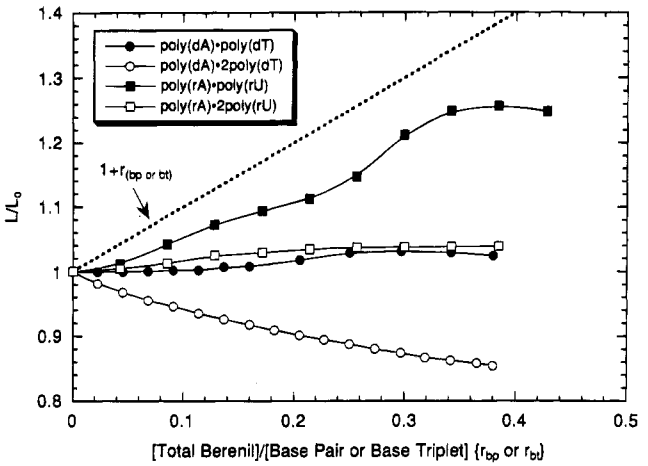


FIGURE 6: Viscometric berenil titrations at 24.7 °C of poly(dA)•poly(dT) (●); poly(dA)•2poly(dT) (○); poly(rA)•poly(rU) (■); and poly(rA)•2poly(rU) (□). $L/L_o$ is the relative contour length of the host structure and is defined in the text. The dashed line reflects the theoretical curve $[1 + r_{(bp\ or\ bt)}]$ predicted by the classic model for intercalation into a rod-like nucleic acid molecule (Lerman, 1961; Cohen & Eisenberg, 1969). Solution conditions are the same as those described in the legend of Figure 3.

host duplexes studied here. Due to the salt-sensitive character of berenil binding to the poly(rA)•poly(rU) RNA duplex and the poly(rA)•2poly(rU) RNA triplex, the viscosity titrations with these two RNA structures had to be performed at a lower ionic strength (35 mM $Na^+$) compared with the 310 mM $Na^+$ used for the viscosity titrations on the corresponding two DNA structures. Note that, upon addition of berenil, the apparent molecular length of the poly(dA)•poly(dT) DNA duplex remains essentially unchanged up to a $r_{bp}$ ratio of 0.16 and then increases very slightly, reaching a plateau at a $r_{bp}$ ratio of 0.25. As we previously have reported (Pilch et al., 1995), this molecular length profile suggests that *berenil binds the poly(dA)•poly(dT) DNA duplex nonintercalatively*. Further inspection of Figure 6 reveals that the molecular length of the poly(dA)•2poly(dT) DNA triplex decreases upon addition of berenil. This molecular length profile also is consistent with *berenil binding to the poly(dA)•2poly(dT) triplex nonintercalatively*. However, we cannot eliminate the alternative possibility of competing viscometric effects between two binding events, such that berenil intercalates into the poly(dA)•poly(dT) and/or poly(dA)•2poly(dT) structures, while a binding-induced conformational change results in a decrease in molecular length that either compensates or overcomes the increase caused by drug intercalation. In fact, the observed decrease in apparent length of the poly(dA)•2poly(dT) DNA structure may reflect a berenil-induced conformational change in the triplex. Such a conformational change could arise from a berenil-induced kink or bend in the helix, thereby reducing its effective molecular length. Alternatively, a conformational change could result from a berenil-induced reduction in the axial ratio of the triplex, which also would act to reduce its solution viscosity.

In a previous viscometric study designed to probe the interaction of the intercalating ligand ethidium bromide with the poly(dA)•2poly(dT) DNA triplex, Scaria & Shafer (1991) observed an initial decrease and subsequent increase in solution viscosity, eventually reaching a plateau. These authors suggest that the initial decrease in solution viscosity may reflect a drug-induced conformational change in the triplex, while ascribing the subsequent increase in solution viscosity to the effects of intercalation. We observe a similar viscosity profile (not shown) when repeating their measurement under the experimental conditions used in our studies (i.e., 310 mM $Na^+$ and 24.7 °C). Inspection of Figure 6 reveals that, unlike the behavior of poly(dA)•2poly(dT) upon addition of ethidium bromide, the solution viscosity of this triplex steadily decreases upon addition of berenil, suggesting little or no contribution from an intercalative mode of binding.

Further inspection of Figure 6 reveals that *the poly(rA)•poly(rU) RNA duplex undergoes a substantial increase in apparent contour length upon addition of berenil, an observation suggestive of some degree of berenil intercalation at 35 mM $Na^+$*. By contrast, addition of berenil to the poly(rA)•2poly(rU) RNA triplex is accompanied by only a slight increase in apparent molecular length. This contour length profile suggests that *berenil binds the poly(rA)•2poly(rU) RNA triplex nonintercalatively, consistent with a minor groove-directed mode of binding*. Thus, for the RNA structures, the presence of a major groove-bound third strand exerts a profound affect on the mode by which berenil interacts with the poly(rA)•poly(rU) RNA duplex. Although both poly(rA)•poly(rU) and poly(rA)•2poly(rU) adopt global A-like conformations, fiber diffraction studies by Arnott et al. (1973, 1976) reveal some key differences between the two structures with respect to several helical parameters, including differences in axial rise per residue, pitch height, and base pair tilt. These structural differences may account for the differential viscometrically detected modes of binding that berenil exhibits when complexed with poly(rA)•poly(rU) and poly(rA)•2poly(rU). The slight increase in solution viscosity that is observed in the contour length profile of the poly(rA)•2poly(rU) RNA triplex may simply reflect a binding-induced increase in the stiffness of the triplex. Once again, however, we cannot rule out the alternative possibility of a fortuitous compensation in which berenil intercalates into the poly(rA)•2poly(rU) RNA triplex, while a binding-induced conformational change results in a decrease in contour length that compensates most of the increase caused by drug intercalation.

Recall that, under identical solution conditions, berenil binding to the poly(rA)•poly(rU) RNA duplex and the poly(rA)•2poly(rU) RNA triplex exhibits similar binding affinities (see Table 2) and similar apparent binding site sizes (i.e., similar saturation binding densities; see Table 1). Despite these similarities, the viscometric profiles of Figure 6 are consistent with berenil binding to the RNA duplex with some degree of intercalation, while binding nonintercalatively to the RNA triplex. Taken together, these observations suggest that berenil, at least in part, intercalates into a RNA duplex, while binding to the minor groove of a RNA triplex. Note that classic intercalative binding, such as that exhibited by ethidium bromide, generally is associated with a binding site size of only two to three base pairs or base triplets (Neidle & Abraham, 1984; Scaria & Shafer, 1991), in contrast to the 5.2 base pair site size we observe for berenil binding to the RNA duplex. We suggest two possible explanations for this apparent discrepancy. First, berenil binding to the RNA duplex may induce an allosteric conformational change in the duplex which, in turn, only allows drug binding at intervals of approximately five base pairs. A second possible explanation for the large apparent binding site envisions

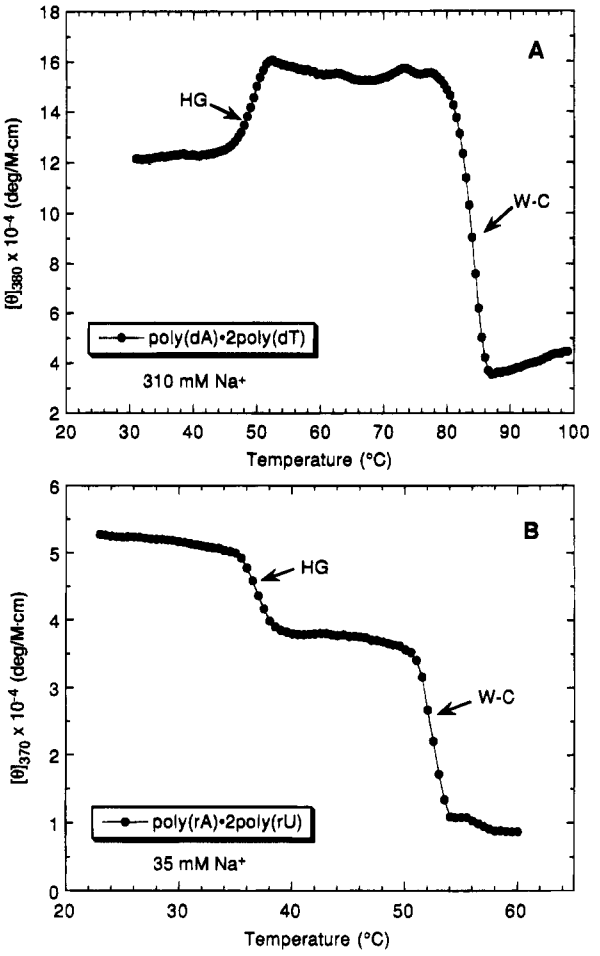


FIGURE 7: CD melting profiles for the berenil–poly(dA)•2poly(dT) complex ($1/r_{bt}$ = 21.7) at 380 nm (A) and for the berenil–poly(rA)•2poly(rU) complex ($1/r_{bt}$ = 5.4) at 370 nm (B). Molar ellipticities, [$\theta$], are in units of deg/M•cm, where M refers to moles of total berenil per liter. Solution conditions are the same as those described in the legend of Figure 3.

berenil only partially intercalating into the RNA duplex, with a portion of the drug protruding out of the helix interior, thereby sterically inhibiting the binding of other drug molecules at neighboring sites.

In the preceding sections, we described our use of CD, absorbance, and viscometric measurements to characterize the triplex-binding properties of berenil. In the sections that follow, we describe our use of calorimetric techniques to characterize the energetics of triplex melting as well as the energetics of berenil binding to the triplex structures. We begin, however, with a description of temperature-dependent CD measurements which allow us to define the appropriate solution conditions for our subsequent calorimetric studies.

*Berenil Remains Bound as the Triplex Melts to the Corresponding Duplex State.* Figure 7 shows the CD melting profiles (at 370 or 380 nm) for the complexes of berenil with the two triplex structures studied here. Note that HG transitions (thermally induced third strand expulsions) also are detected at these wavelengths, an observation which demonstrates the persistence of an induced CD signal from the bound drug as either the DNA or the RNA triplex melts to the corresponding duplex state. The persistence of these induced CD signals suggests that, *within the temporal window accessible to CD, berenil remains bound to either the DNA or RNA duplex [poly(dA)•poly(dT) or poly(rA)•poly(rU)] upon dissociation of the relevant third strand [poly(dT) or poly(rU)].* These results, coupled with those derived from the UV melting profiles presented in Figure 2, allow us to define the conditions necessary to conduct calorimetric studies of the energetics associated with berenil–triplex interactions, as well as the effects of berenil binding on the energetics of triplex melting. These calorimetric studies are described below.

*Berenil Binding Increases the Enthalpy of the Triplex to Duplex Transition.* We used DSC to measure the enthalpy change associated with the Hoogsteen (HG) triplex to duplex transitions in both the presence and absence of bound berenil. Panels A and B of Figure 8 show the DSC profiles of the poly(dA)•2poly(dT) DNA triplex in its berenil-free and berenil bound (at $r_{bt}$ = 0.30) states, respectively. The enthalpy data derived from integration of the low temperature peaks (the HG transitions) are listed Table 3. Note that, when berenil is bound, the DNA triplex to duplex transition is more endothermic (6.0 kcal/mol) than it is in the absence of berenil (4.1 kcal/mol). Recall that our viscometric studies (Figure 6) are consistent with berenil binding in the minor groove of the poly(dA)•2poly(dT) DNA triplex. These collective results suggest that minor groove-bound berenil and the major groove-bound third strand [poly(dT) in this case] influence each other energetically. We (Park & Breslauer, 1992) previously have observed such energetic cross-talk between the occupants of the major and minor grooves when the poly(dA)•2poly(dT) DNA triplex served as the host structure for binding by the minor groove-directed ligand netropsin.

Panels C and D of Figure 8 show the DSC profiles for the poly(rA)•2poly(rU) RNA triplex in its berenil-free and berenil-bound (at $r_{bt}$ = 0.21) states, respectively. Table 3 lists the enthalpy data derived from integration of the low temperature HG peaks. Note that, for the berenil-bound state (panel D of Figure 8), the WC high temperature transition exhibits a small shoulder. We believe that this shoulder corresponds to a small degree of secondary binding that occurs at $r_{bp}$ = 0.21 [that mode of binding corresponding to an apparent site size of 1.7 ($r_{bp}$ = 0.59); see Table 1]. Inspection of the data in Table 3 reveals that, as with the DNA structures, the RNA triplex to duplex transition also requires a greater enthalpic input when berenil is bound, although the difference is much less pronounced (2.4 versus 2.0 kcal/mol) than when the corresponding DNA triplex serves as the host. Recall that our viscometric studies (Figure 6) are consistent with berenil binding to the poly(rA)•2poly(rU) RNA triplex by a non-intercalative mode (e.g., minor groove binding). Hence, as was observed in the berenil-poly(dA)•2poly(dT) DNA complex, energetic cross-talk between occupants of the major [the poly(rU) third strand] and minor (bound berenil) grooves also occurs in the berenil–poly(rA)•2poly(rU) RNA complex. However, the extent of such energetic groove cross-talk appears to be reduced in the RNA triplex relative to the DNA triplex. Conformational differences between the poly(dA)•2poly(dT) DNA triplex and poly(rA)•2poly(rU) RNA triplex may contribute, in part, to this differential degree of energetic groove cross-talk.

*Berenil Binding to the DNA and RNA Triplexes Is Enthalpically More Favorable Than Berenil Binding to the Corresponding Duplexes.* We used isothermal titration calorimetry to measure the binding enthalpies for berenil

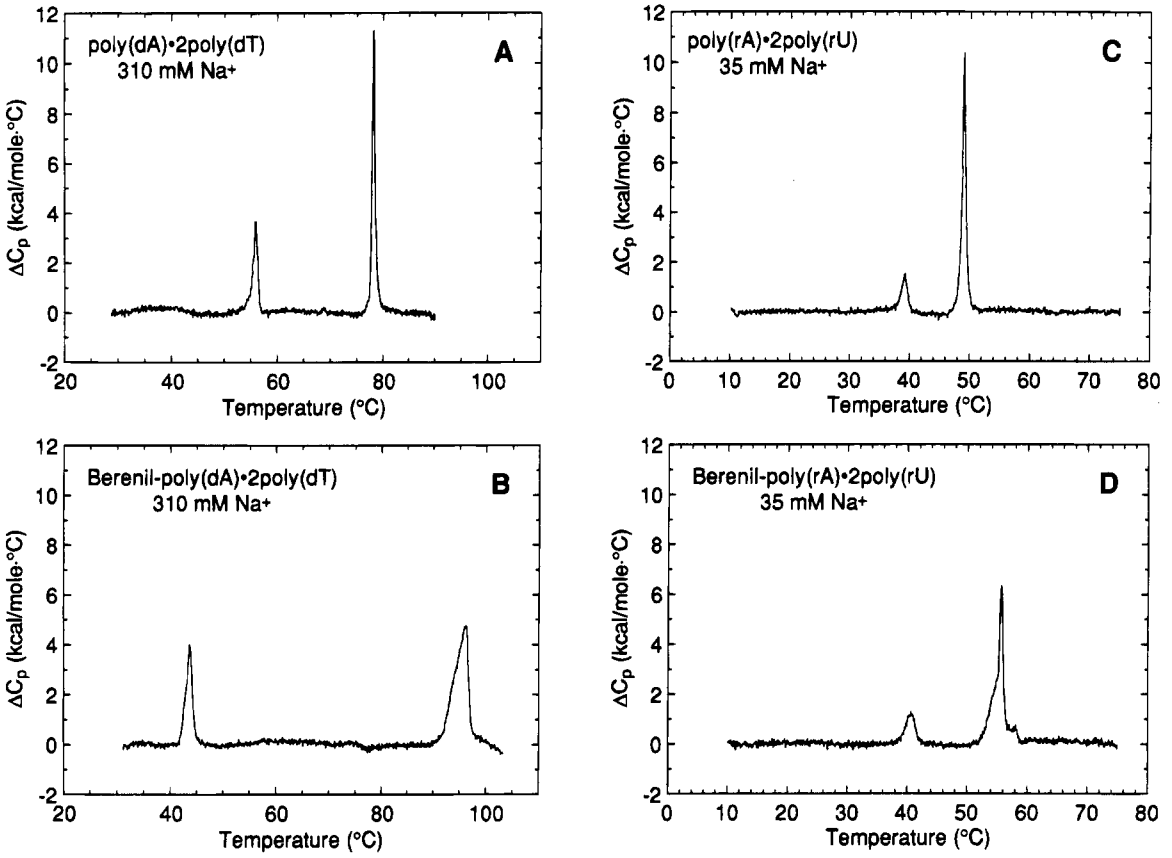


FIGURE 8: Excess heat capacity ($\Delta C_p$) versus temperature profiles for poly(dA)•2poly(dT) (A); the berenil−poly(dA)•2poly(dT) complex ($r_{bt}$ = 0.30) (B); poly(rA)•2poly(rU) (C); and the berenil−poly(rA)•2poly(rU) complex ($r_{bt}$ = 0.21) (D). Nucleic acid concentrations were 0.3 mM in base triplet. Solution conditions are the same as those described in the legend of Figure 3.

Table 3: Calorimetric and van't Hoff Transition Enthalpies for the Berenil-Free and Berenil-Saturated Poly(dA)•2Poly(dT) and Poly(rA)•2Poly(rU) Triplexes and for the Corresponding Berenil-Free and Berenil-Saturated Poly(dA)•Poly(dT) and Poly(rA)•Poly(rU) Duplexes[a]

| transition | $r_{bt}$ or $r_{bp}$ | $\Delta H_{cal}$[b] (kcal/mol bt or bp) | $\Delta H_{vH}$[c] (kcal/mol bt or bp) | $\Delta H_{vH}/\Delta H_{cal}$ (cooperative unit) |
|---|---|---|---|---|
| DNA | | | | |
| dA•2(dT) → dA•dT + dT | 0 | 4.1 | 192 | 47 |
| dA•2(dT) → dA•dT + dT | 0.30 | 6.0 | 181 | 30 |
| dA•dT → dA + dT | 0 | 10.4 | 260 | 25 |
| dA•dT → dA + dT | 0.23 | 14.8 | 276 | 19 |
| RNA | | | | |
| rA•2(rU) → rA•rU + rU | 0 | 2.0 | 173 | 87 |
| rA•2(rU) → rA•rU + rU | 0.21 | 2.4 | 172 | 72 |
| rA•rU → rA + rU | 0 | 8.7 | 269 | 31 |
| rA•rU → rA + rU | 0.19 | 8.8 | 232 | 26 |

[a] The DNA data were measured at 310 mM $Na^+$, while the RNA data were measured at 35 mM $Na^+$. [b] Calorimetric transition enthalpies ($\Delta H_{cal}$) were calculated from the areas under $\Delta C_p$ vs temperature curves, with an uncertainty in the data of <5%. [c] The van't Hoff transition enthalpies ($\Delta H_{vH}$) were calculated from the shapes of the first derivatives of UV melting curves, with an assumed molecularity of 1 (Marky & Breslauer, 1987) and an uncertainty in the data of <10%.

Table 4: Binding Enthalpies for Berenil Complexation with the Poly(dA)•2Poly(dT) and Poly(rA)•2Poly(rU) Triplexes and with the Corresponding Poly(dA)•Poly(dT) and Poly(rA)•Poly(rU) Duplexes[a]

| host nucleic acid | [$Na^+$] (mM) | $\Delta H_B$[b] (kcal/mol) |
|---|---|---|
| poly(dA)•poly(dT) | 310 | −2.3 ± 0.4 |
| poly(dA)•2poly(dT) | 310 | −4.3 ± 0.4 |
| poly(rA)•poly(rU) | 35 | −3.0 ± 0.6 |
| poly(rA)•2poly(rU) | 35 | −5.0 ± 0.5 |

[a] Experimental conditions are as stated in the footnote of Table 1. [b] $\Delta H_B$ is the enthalpy of berenil binding to the host nucleic acid, as measured directly in titration calorimetry experiments. In all cases, binding enthalpies were determined at $1/r_{bp}$ or $1/r_{bt}$ values of 29.1 and are expressed in units of kcal/mol of injected berenil. Errors reflect single standard deviations from multiple electronic calibration experiments, in which the heat pulses were similar in magnitude to the experimentally measured heats.

complexation with the poly(dA)•2poly(dT) and poly(rA)•2poly(rU) triplexes and with the corresponding poly(dA)•poly(dT) and poly(rA)•poly(rU) duplexes. These measurements were conducted at 25 °C under solution conditions which ensured that the duplexes and triplexes were fully formed in both their drug-free and drug-bound states (310 mM $Na^+$ for the DNA measurements and 35 mM $Na^+$ for the RNA measurements). The binding enthalpies derived from these measurements are listed in Table 4. Note that berenil binding to the poly(dA)•2poly(dT) triplex is 1.9 times more exothermic (favorable) than berenil binding to the poly(dA)•poly(dT) duplex (−4.3 versus −2.3 kcal/mol). Third strand-induced changes in the electron densities and topologies of the functional groups which line the minor groove may contribute, in part, to these differential binding enthalpies. Recall that our viscometric studies (Figure 6) are consistent with berenil binding nonintercalatively (e.g., to the minor groove) to both DNA structures. Thus, occupancy of the major groove by the third strand [poly(dT)] influences the energetics of berenil binding in the minor groove, providing yet another manifestation of energetic cross-talk between the major and minor grooves. This conclusion is consistent with the results of our DSC studies in which we

examined the effects of berenil binding on third strand denaturation and highlights the potential usefulness of minor groove-directed ligands to modulate the energetics of triplex formation.

Further inspection of the data in Table 4 reveals that berenil binding to the poly(rA)·2poly(rU) RNA triplex is 1.7 times more exothermic (favorable) than berenil binding to the poly(rA)·poly(rU) RNA duplex (−5.0 versus −3.0 kcal/mol). Recall that our viscometric studies (Figure 6) are consistent with berenil binding nonintercalatively (e.g., to the minor groove) to the RNA triplex, while intercalating into the corresponding duplex. Collectively, these observations suggest that berenil binding to the minor groove of the RNA triplex is enthalpically more favorable than berenil intercalation into the corresponding RNA duplex.

*The Enhanced Berenil Binding Enthalpy for the Triplex State Is Offset by a Loss in Binding Entropy.* Application of the standard thermodynamic relationship

$$\Delta G^\circ = -RT \ln K_{app} \quad (7)$$

to the apparent DNA binding constants derived in our Benesi−Hildebrand analyses (see Table 2) indicates that the free energy of berenil binding to the poly(dA)·2poly(dT) DNA triplex is less favorable ($\Delta G^\circ$ at 25 °C = −7.3 kcal/mol) than for berenil binding to the poly(dA)·poly(dT) DNA duplex ($\Delta G^\circ$ at 25 °C = −9.0 kcal/mol). However, our isothermal titration calorimetric measurements reveal that berenil binding to the poly(dA)·2poly(dT) DNA triplex is more exothermic than berenil binding to the poly(dA)·poly(dT) DNA duplex. Thus, the more favorable binding enthalpy that berenil exhibits for the DNA triplex state (in which the major groove is occupied) is more than offset by a substantial loss in binding entropy ($\Delta S$ = +10 eu for berenil binding to the triplex and +23 eu for berenil binding to the duplex). In other words, the energetic cross-talk between the occupants of the major and minor grooves has compensating enthalpic and entropic components. Such enthalpy−entropy compensations are quite common in drug−nucleic acid interactions (Breslauer et al., 1987).

Similarly, with the RNA structures, we find that berenil binding to the poly(rA)·2poly(rU) triplex is slightly less energetically favorable than berenil binding to the poly(rA)·poly(rU) duplex ($\Delta G$ at 25 °C = −7.0 versus −7.5 kcal/mol). As with the DNA structures, the enthalpy berenil gains by binding to the RNA triplex (nonintercalatively) relative to that which it exhibits when binding to the RNA duplex (intercalatively) is offset by a loss of binding entropy ($\Delta S$ = +6.7 eu for berenil binding to the triplex and +8.4 eu for berenil binding to the duplex). Hence, enthalpy−entropy compensations arise not only when comparing the ligand−nucleic acid complexes formed by ligands with similar modes of binding but also when comparing those formed by ligands with differing modes of binding.

*Berenil Binding Decreases the Cooperativity of Triplex Melting.* As noted above, we used DSC to measure, in both the presence and absence of bound berenil, the enthalpy change ($\Delta H_{cal}$) associated with the HG transitions (the third strand expulsions) of the poly(dA)·2poly(dT) and poly(rA)·2poly(rU) triplexes. We also have derived the corresponding van't Hoff transition enthalpies ($\Delta H_{vH}$) from analysis of the shapes of the first derivatives of the UV melting profiles, assuming a molecularity of 1 due to the pseudomonomolecular nature of the transitions. For each transition, the ratio of $\Delta H_{vH}$ to $\Delta H_{cal}$ provides a measure of the cooperativity of the melting event (Breslauer et al., 1992). These data are summarized in Table 3. Inspection of these data reveals that, in the presence of bound berenil, the HG transitions of both the poly(dA)·2poly(dT) and poly(rA)·2poly(rU) triplexes exhibit cooperative units of 30 and 72 base triplets, respectively, while the berenil-free DNA and RNA triplexes exhibit cooperative units of 47 and 87 base triplets, respectively. Once again, recall that our viscometric measurements are consistent with berenil binding in the minor groove of both triplex structures. Thus, occupancy of the minor groove by berenil decreases the cooperativity of the melting event associated with expulsion of the major groove-bound third strand, a phenomenon we previously have observed when the poly(dA)·2poly(dT) DNA triplex serves as the host structure for the minor groove-binding ligand netropsin (Park & Breslauer, 1992). Consequently, in addition to the enthalpic cross-talk we observe between the two grooves in the DNA triplex (as reflected in the relevant binding enthalpies listed in Table 4), we also observe groove cross-talk with respect to melting cooperativity in both the DNA and RNA triplexes.

For comparative purposes, Table 3 also includes the corresponding enthalpy data for the melting of the poly(dA)·poly(dT) and poly(rA)·poly(rU) duplexes in the presence and absence of bound berenil. Note that berenil binding also decreases the cooperativity of duplex melting, an observation previously noted in this laboratory in studies probing the interactions of both minor groove-directed and intercalating ligands with various RNA and DNA host duplexes (Marky et al., 1983a,b; Chou et al., 1987; Chou, 1990; Park & Breslauer, 1992; Park, 1992).

## CONCLUDING REMARKS

We have used a combination of spectroscopic, calorimetric, and viscometric techniques to demonstrate that, under appropriate conditions, berenil can bind to both DNA and RNA triplexes and that these binding events exhibit properties characteristic of minor groove binding. We also have shown that bound berenil influences the thermal stability, melting energetics, and melting cooperativities of both a DNA and a RNA host triplex. Furthermore, our data reveal a substantial degree of cross-talk between occupants of the major and minor grooves, a phenomenon that highlights the potential use of minor groove-directed ligands to modulate the affinities and specificities of third strands for their duplex targets. Such knowledge is required for the ultimate development of a more rational approach to the design of drugs aimed at enhancing the efficacy of antisense and/or antigene therapeutic strategies. Significantly, however, independent of such potential applications, our data provide fundamental insight into the differential recognition of DNA and RNA duplex and triplex structures by berenil, a pharmacologically active ligand.

## ACKNOWLEDGMENT

We thank Dr. George Strauss, in whose lab the viscometry experiments were conducted, Robert Porcja for assistance with setting up the viscometry apparatus, and Dr. G. Eric Plum for helpful discussions.

## APPENDIX

In our previous article (Pilch et al., 1995), we used the Appendix to present data which mapped the influence of berenil binding on the phase diagram of a duplex host structure. In this Appendix, we present data which map the influence of berenil binding on the phase diagrams of two triplex host structures.

*The Influence of Berenil Binding on the Poly(dA)·2Poly(dT) Phase Diagram.* Riley et al. (1966) previously have determined a phase diagram for the poly(dA)·2poly(dT) DNA triplex in the absence of drug binding. Specifically, they mapped the salt dependence of the thermal stabilities ($T_m$) of the following three transitions:

poly(dA)·2poly(dT) ⇌
poly(dT) + poly(dA)·poly(dT) [HG]

poly(dA)·poly(dT) + poly(dT) ⇌
poly(dA) + 2poly(dT) [WC]

poly(dA)·2poly(dT) ⇌
poly(dA) + 2poly(dT) [TSS]

where TSS denotes the triplex to single strand transition. In the paragraphs that follow, we describe how we have expanded their phase diagram by evaluating how these three equilibria are influenced by berenil binding. Such expanded phase diagrams are important for meaningfully defining and comparing nucleic acid binding properties over a range of solution conditions.

Panel A of Figure A1 shows the effect of berenil binding on the salt dependence of the thermal stability of the poly(dA)·2poly(dT) triplex. Note that, at $r_{bt}$ ratios $\leq 0.092$, a triple point occurs at $\approx$1010 mM $Na^+$ (log [$Na^+$] = 0.004) while, at $r_{bt}$ ratios $\geq 0.18$, the triple point shifts to a higher $Na^+$ concentration of $\approx$1260 mM $Na^+$ (log [$Na^+$] = 0.100). Inspection of panel A reveals that, at $Na^+$ concentrations below the triple points {1010 mM $Na^+$ (log [$Na^+$] = 0.004) or 1260 mM $Na^+$ (log [$Na^+$] = 0.100)}, berenil addition causes the $T_m$ values of the WC transitions (II → I) to increase. Furthermore, the slopes of the lines, $\partial T_m/\partial$ log [$Na^+$], that separate regions I and II (which correspond to the WC transitions) are quite different for the drug-free and drug-bound duplexes, (19.3 °C for the drug-free duplex and 0.3 °C for the drug-bound duplex at $r_{bt}$ = 0.46). It is gratifying to note that the $\partial T_m/\partial$ log [$Na^+$] values we have determined for the WC transitions of poly(dA)·2poly(dT) in the absence of drug are consistent with previously reported values (Riley et al., 1966; Marky et al., 1985; Klump, 1988; Park, 1992).

Further inspection of panel A reveals that, in contrast to the effect of berenil binding on the $T_m$ values of the WC transitions, addition of berenil at $Na^+$ concentrations below the triple points {1010 mM $Na^+$ (log [$Na^+$] = 0.004) or 1260 mM $Na^+$ (log [$Na^+$] = 0.100)} but above 125 mM $Na^+$ (log [$Na^+$] = −0.903) causes the $T_m$ values of the HG transitions (III → II) to decrease. However, at $Na^+$ concentrations below 90 mM (log [$Na^+$] = −1.050), berenil binding causes the $T_m$ values of the HG transitions to increase. Between the $Na^+$ concentrations of 90 and 125 mM, berenil binding causes the $T_m$ of the HG transitions to decrease at $r_{bt}$ ratios <0.092, while causing them to increase at $r_{bt}$ ratios >0.18. This observation is consistent with differential contributions

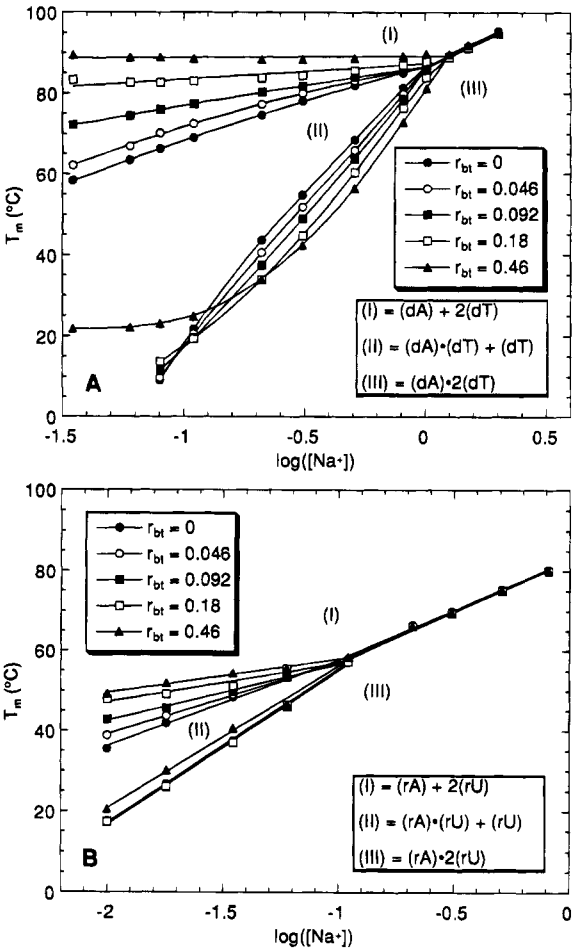


FIGURE A1: Phase diagrams which map $T_m$ versus log [$Na^+$] for the poly(dA)·2poly(dT) DNA triplex (A) and the poly(rA)·2poly(rU) RNA triplex (B) and their complexes with berenil at the indicated values of $r_{bt}$. The structural states which correspond to each phase (I, II, or III) are indicated. Buffer conditions were 10 mM sodium cacodylate (pH 6.8−6.9) and 0.1 mM EDTA.

to triplex thermal stability from the two apparent binding events which berenil exhibits when complexed with the poly(dA)·2poly(dT) triplex (see Table 1). Within the $Na^+$ concentration range of 210 to 1010 mM, note that the slopes of the lines which separate regions II and III (the HG transitions) are similar for the drug-free and drug-bound triplexes (ranging from 69.2 to 76.0 °C). This observation contrasts with the behavior of the WC transition lines (separating regions I and II) for the drug-free and drug-bound triplexes. The $\partial T_m/\partial$ log [$Na^+$] values we observe for the HG transition lines of the drug-free and drug-bound poly(dA)·2poly(dT) triplex are consistent with those reported previously in the absence of added drug for the HG transitions of the poly(dA)·2poly(dT) polymeric triplex (Riley et al., 1966; Park, 1992) and the $d(T)_{19}$·$d(A)_{19}$·$d(T)_{19}$ oligomeric triplex (Kibler-Herzog et al., 1990).

The phase diagram (Figure A1, panel A) also reveals that, at $Na^+$ concentrations above the triple points {1010 mM $Na^+$ (log [$Na^+$] = 0.004) or 1260 mM $Na^+$ (log [$Na^+$] = 0.100)}, the transition lines overlap. Thus, berenil binding has virtually no effect on the $T_m$ values of the TSS (phase III → phase I) transitions. The slopes of the phase diagram lines separating regions I and III (which correspond to the TSS transitions) are similar for the drug-free and drug-bound triplexes, ranging from 27.4 to 29.5 °C. Once again, it is gratifying to note that these $\partial T_m/\partial$ log [$Na^+$] values are

Table A1: Salt-Dependent Thermodynamic Data for the Melting of the Berenil-Free and Berenil-Saturated Poly(dA)·2Poly(dT) and Poly(rA)·2Poly(rU) Triplexes

| transition | $r_{bt}$ | $\Delta H_{cal}$[a] (kcal/mol nucleotide) | $\partial T_m/\partial \log [Na^+]$[b] (°C) | $\Delta i$[c] |
|---|---|---|---|---|
| | | Poly(dA)·2Poly(dT) | | |
| HG | 0 | 1.4 | 71.2 | 0.20 |
| HG | 0.30 | 2.0 | 76.0 | 0.33 |
| WC | 0 | 4.6 | 19.3 | 0.16 |
| WC | 0.30 | 6.7 | 0.3 | 0.003 |
| | | Poly(rA)·2Poly(rU) | | |
| HG | 0 | 0.67 | 37.1 | 0.056 |
| HG | 0.21 | 0.80 | 37.0 | 0.067 |
| WC | 0 | 4.5 | 22.9 | 0.22 |
| WC | 0.21 | 5.0[d] | 8.0 | 0.083[d] |

[a] Calorimetric transition enthalpies ($\Delta H_{cal}$) were calculated from the areas under $\Delta C_p$ vs temperature curves, with an uncertainty in the data of <5%. The poly(dA)·2poly(dT) data were measured at 310 mM $Na^+$, while the poly(rA)·2poly(rU) data were measured at 35 mM $Na^+$. [b] The UV melting studies on the poly(dA)·2poly(dT) triplex were conducted at $Na^+$ concentrations between 210 and 810 mM, while those on the poly(rA)·2poly(rU) triplex were conducted between $Na^+$ concentrations of 10 and 60 mM. [c] $\Delta i$ denotes the thermodynamic degree of ion dissociation and was calculated according to eq A1. [d] $\Delta H_{cal}$ corresponding to the WC transition of the berenil–poly(rA)·2poly(rU) complex at $r_{bt}$ = 0.21 includes a contribution of approximately 0.5 kcal/mol nucleotide from a small amount of secondary berenil binding to the poly(rA)·poly(rU) duplex, as reflected by the presence of a small shoulder on the high-temperature (WC) peak of the DSC profile in panel D of Figure 8. This contribution also is reflected in the corresponding value for $\Delta i$.

consistent with those observed previously by Klump (1988) for the TSS transition of the poly(dA)·2poly(dT) triplex in the absence of added drug.

To normalize comparisons of $\partial T_m/\partial \log [Na^+]$ values for differences in transition enthalpies ($\Delta H$), one must calculate the thermodynamic degree of ion dissociation ($\Delta i$) for each transition (Record et al., 1976, 1978) by

$$\Delta i = \frac{\partial T_m}{\partial \log [Na^+]}\left[\frac{\Delta H}{2.3R(T_m)^2}\right] \qquad \text{(A1)}$$

Using the calorimetric transition enthalpies derived from our DSC profiles (panels A and B of Figure 8) and $\partial T_m/\partial \log [Na^+]$ values derived from the appropriate UV melting profiles acquired at $Na^+$ concentrations between 210 and 810 mM, we have derived $\Delta i$ values for the HG and WC transitions of the berenil-free and berenil-saturated (at $r_{bt}$ = 0.30) states of the poly(dA)·2poly(dT) triplex. The results of these calculations are summarized in Table A1. Inspection of these data reveals that thermal expulsion of the poly(dT) third strand from the poly(dA)·poly(dT) duplex (the HG transition) only exhibits a relatively small difference in the degree of ion dissociation in the absence (0.20) and in the presence (0.33) of bound berenil. This observation suggests that the net difference in the electrostatic environment between the triplex and duplex plus single-stranded states is similar for both the drug-free and drug-bound triplexes.

Further inspection of the data in Table A1 reveals that thermal denaturation of the remaining poly(dA)·poly(dT) duplex (the WC transition) is associated with markedly different degrees of ion dissociation in the absence (0.16) and presence (0.003) of bound berenil. This observation suggests that, unlike the net difference in electrostatic environment between the triplex and duplex plus single-stranded states, the net difference in the electrostatic environment between the duplex and single-stranded states differs markedly for the drug-free and drug-saturated duplex states.

*The Influence of Berenil Binding on the Poly(rA)·2Poly(rU) Phase Diagram.* Krakauer and Sturtevant (1968) previously have determined a phase diagram for the poly(rA)·2poly(rU) triplex in the absence of drug binding. Their phase diagram mapped the salt dependence of the thermal stabilities of the following three transitions:

$$\text{poly(rA)·2poly(rU)} \rightleftharpoons \text{poly(rA)·poly(rU)} + \text{poly(rU)} \qquad \text{[HG]}$$

$$\text{poly(rA)·poly(rU)} + \text{poly(rU)} \rightleftharpoons \text{poly(rA)} + 2\text{poly(rU)} \qquad \text{[WC]}$$

$$\text{poly(rA)·2poly(rU)} \rightleftharpoons \text{poly(rA)} + 2\text{poly(rU)} \qquad \text{[TSS]}$$

In the paragraphs that follow, we describe how we have expanded their phase diagram by evaluating how these three equilibria are influenced by berenil binding.

Panel B of Figure A1 shows the effect of berenil binding on the phase diagram of the poly(rA)·2poly(rU) triplex. Note that this expanded phase diagram exhibits a triple point at ≈110 mM $Na^+$ (log $[Na^+] = -0.96$) At $Na^+$ concentrations below the triple point, addition of berenil causes the $T_m$ values of the WC transitions (II → I) to increase. Furthermore, the slopes of the lines that separate regions I and II (which correspond to the WC transitions) are quite different for the drug-free and drug-bound duplexes (22 °C for the drug-free duplex and 8.0 °C for the drug-bound duplex at $r_{bp}$ = 0.46). It is gratifying to note that the $\partial T_m/\partial \log [Na^+]$ values we have determined in the absence of drug for the WC transitions of poly(rA)·poly(rU) are consistent with values previously reported by us and others (Krakauer & Sturtevant, 1968; Record et al., 1976; Chou, 1990; Pilch et al., 1995).

Further inspection of panel B in Figure A1 reveals that, in contrast to the effect of berenil binding on the $T_m$ values of the WC transitions, addition of berenil at $Na^+$ concentrations below the triple point {110 mM $Na^+$ (log $[Na^+] = -0.96$)} and at $r_{bt}$ ratios ≤ 0.18 causes the $T_m$ values of the HG transitions (III → II) to decrease very slightly ($\Delta T_m$ ranges from −0.2 to −0.6 °C). However, addition of berenil at $Na^+$ concentrations below the triple point {110 mM $Na^+$ (log $[Na^+] = -0.96$)} and at $r_{bt}$ ratios ≥ 0.18 causes the $T_m$ values of the HG transitions to increase. This observation may reflect the thermally stabilizing effects of electrostatically driven secondary binding (e.g., drug stacking on the triplex exterior) at high $r_{bt}$ ratios. Note that the slopes of the lines that separate regions II and III (which correspond to the HG transitions) are virtually identical for the drug-free and drug-bound (at $r_{bt}$ ratios ≤ 0.18) triplexes, ranging from 37.1 °C for the drug-free triplex to 37.0 °C for the drug-bound triplex at $r_{bp}$ = 0.18. These $\partial T_m/\partial \log [Na^+]$ values also are consistent with those previously reported for the HG transition of the poly(rA)·2poly(rU) triplex in the absence of added drug (Krakauer & Sturtevant, 1968; Record et al., 1976).

The phase diagram in panel B also reveals that, at $Na^+$ concentrations above the triple point {110 mM $Na^+$ (log $[Na^+] = -0.96$)}, the transition lines overlap. Thus, berenil

binding has virtually no effect on the $T_m$ values of the TSS (phase III → phase I) transitions. The average slope of the lines corresponding to the TSS transitions in the presence and absence of drug is 25.2 °C. This value is in agreement with those previously reported by us and others for the TSS transition of this triplex in the presence and/or absence of added berenil (Krakauer & Sturtevant, 1968; Record et al., 1976; Pilch et al., 1995).

Once again, to normalize our comparisons of the $\partial T_m/\partial \log [Na^+]$ values for differences in transition enthalpies, we used the calorimetric transition enthalpies derived from the DSC profiles shown in panels C and D of Figure 8, the $\partial T_m/\partial \log [Na^+]$ values derived from the appropriate UV melting profiles acquired at $Na^+$ concentrations between 10 and 60 mM, and eq A1 to calculate $\Delta i$ values for the HG and WC transitions of the berenil-free and berenil-saturated (at $r_{bt} = 0.21$) states of the poly(rA)·2poly(rU) RNA triplex. These values are summarized in Table A1. Inspection of these data reveals that thermal expulsion of the poly(rU) third strand from the poly(rA)·poly(rU) duplex (the HG transition) only exhibits a relatively small difference between the degree of ion dissociation in the absence (0.056) and in the presence (0.067) of bound berenil, while thermal denaturation of the remaining duplex (the WC transition) is associated with markedly differing degrees of ion dissociation in the absence (0.22) and presence (0.083) of bound berenil. Thus, as noted when comparing the salt-dependent thermodynamic data for the melting of the berenil-free and berenil-saturated states of the poly(dA)·2poly(dT) DNA triplex, the net difference in the electrostatic environment between the RNA triplex and RNA duplex plus single-stranded states is similar for both the drug-free and drug-bound forms of the poly(rA)·2poly(rU) triplex, despite the fact that the net difference in the electrostatic environment between the component duplex and single-stranded states differs markedly for these triplexes.

In this Appendix, we have expanded the existing phase diagrams of a DNA and a RNA triplex to include the influence of drug binding. Our data reveal a complex interplay between the influences of salt and drug binding density on the thermal stabilities of the triplex and duplex states. These interdependencies underscore the need for such multiparametric phase diagrams to allow one to meaningfully define and compare the drug binding properties of nucleic acid structures over a range of solution conditions.

## REFERENCES


Arnott, S., & Selsing, E. (1974) *J. Mol. Biol. 88*, 509−521.

Arnott, S., Hukins, D. W. L., Dover, S. D., Fuller, W., & Hodgson, A. R. (1973) *J. Mol. Biol. 81*, 107−122.

Arnott, S., Bond, P. J., Selsing, E., & Smith, P. J. C. (1976) *Nucleic Acids Res. 3*, 2459−2470.

Barceló, F., & Portugal, J. (1993) *Biophys. Chem. 47*, 251−260.

Benesi, H. A., & Hildebrand, J. H. (1949) *J. Am. Chem. Soc. 71*, 2703−2707.

Bloomfield, V. A., Crothers, D. M., & Tinoco, I., Jr. (1974) *Physical Chemistry of Nucleic Acids*, pp 442−445, Harper & Row, New York.

Breslauer, K. J., Remeta, D. P., Chou, W.-Y., Ferrante, R., Curry, J., Zaunczkowski, D., Snyder, J. G., & Marky, L. A. (1987) *Proc. Natl. Acad. Sci. U.S.A. 84*, 8922−8926.

Breslauer, K. J., Freire, E., & Straume, M. (1992) *Methods Enzymol. 211*, 533−567.

Bresloff, J. L., & Crothers, D. M. (1981) *Biochemistry 20*, 3547−3553.

Brown, D. G., Sanderson, M. R., Skelly, J. V., Jenkins, T. C., Brown, T., Garman, E., Stuart, D. I., & Neidle, S. (1990) *EMBO J. 9*, 1329−1334.

Brown, D. G., Sanderson, M. R., Garman, E., & Neidle, S. (1992) *J. Mol. Biol. 226*, 481−490.

Chou, W.-Y. (1990) Ph.D. Thesis, Rutgers University, New Brunswick, NJ.

Chou, W.-Y., Marky, L. A., Zaunczkowski, D., & Breslauer, K. J. (1987) *J. Biomol. Struct. Dyn. 5*, 345−359.

Cohen, G., & Eisenberg, H. (1969) *Biopolymers 8*, 45−55.

Crothers, D. M. (1971) *Biopolymers 10*, 2147−2160.

Durand, M., Thuong, N. T., & Maurizot, J. C. (1992) *J. Biol. Chem. 267*, 24394−24399.

Durand, M., Thuong, N. T., & Maurizot, J. C. (1994) *J. Biomol. Struct. Dyn. 11*, 1191−1202.

Eriksson, S., Kim, S. K., Kubista, M., & Nordén, B. (1993) *Biochemistry 32*, 2987−2998.

François, J. C., Saison-Behmoaras, T., Barbier, C., Chassignol, M., Thuong, N. T., & Hélène, C. (1989) *Proc. Natl. Acad. Sci. U.S.A. 86*, 9702−9706.

Herrera, J. E., & Chaires, J. B. (1989) *Biochemistry 28*, 1993−2000.

Hélène, C. (1991a) *Anti-Cancer Drug Des. 6*, 569−584.

Hélène, C. (1991b) *Eur. J. Cancer 27*, 1466−1471.

Hélène, C., & Toulmé, J.-J. (1990) *Biochim. Biophys. Acta 1049*, 99−125.

Htun, H., & Dahlberg, J. E. (1988) *Science 241*, 1791−1796.

Jenkins, T. C., Lane, A. N., Neidle, S., & Brown, D. G. (1993) *Eur. J. Biochem. 213*, 1175−1184.

Job, P. (1928) *Ann. Chim. (Paris) 9*, 113−134.

Johnston, B. H. (1988) *Science 241*, 1800−1804.

Kibler-Herzog, L., Kell, B., Zon, G., Shinozuka, K., Mizan, S., & Wilson, W. D. (1990) *Nucleic Acids Res. 18*, 3545−3555.

Klump, H. H. (1988) *Can. J. Chem. 66*, 804−811.

Krakauer, H., & Sturtevant, J. M. (1968) *Biopolymers 6*, 491−512.

Lane, A. N., Jenkins, T. C., Brown, T., & Neidle, S. (1991) *Biochemistry 30*, 1372−1385.

Lee, J. S., Latimer, L. J. P., & Hampel, K. J. (1993) *Biochemistry 32*, 5591−5597.

Lehrman, E., & Crothers, D. M. (1977) *Nucleic Acids Res. 4*, 1381−1392.

Lerman, L. S. (1961) *J. Mol. Biol. 3*, 18−30.

Lin, C. H., & Patel, D. J. (1992) *J. Am. Chem. Soc. 114*, 10658−10660.

Lyamichev, V. I., Mirkin, S. M., & Frank-Kamenetskii, M. D. (1986) *J. Biomol. Struct. Dyn. 3*, 667−669.

Marky, L. A., & Breslauer, K. J. (1987) *Biopolymers 26*, 1601−1620.

Marky, L. A., Snyder, J. G., & Breslauer, K. J. (1983a) *Nucleic Acids Res. 11*, 5701−5715.

Marky, L. A., Snyder, J. G., Remeta, D. P., & Breslauer, K. J. (1983b) *J. Biomol. Struct. Dyn. 1*, 487−507.

McGhee, J. D., & von Hippel, P. H. (1974) *J. Mol. Biol. 86*, 469−489.

Mergny, J. L., Collier, D., Rougée, M., Montenay-Garestier, T., & Hélène, C. (1991) *Nucleic Acids Res. 19*, 1521−1526.

Marky, L. A., Curry, J., & Breslauer, K. J. (1985) in *Molecular Basis of Cancer, Part B: Macromolecular Recognition, Chemotherapy, and Immunology* (Rein, R., Ed.) pp 155−173, Alan R. Liss, Inc., New York.

Mergny, J. L., Duval-Valentin, G., Nguyen, C. H., Perrouault, L., Faucon, B., Rougée, M., Montenay-Garestier, T., Bisagni, E., & Hélène, C. (1992) *Science 256*, 1681−1684.

Moser, H. E., & Dervan, P. B. (1987) *Science 238*, 645−650.

Müller, W., & Crothers, D. M. (1968) *J. Mol. Biol. 35*, 251−290.

Neidle, S., & Abraham, Z. (1984) *CRC Crit. Rev. Biochem. 17*, 73−121.

Park, Y.-W. (1992) Ph.D. Thesis, Rutgers University, New Brunswick, NJ.

Park, Y.-W., & Breslauer, K. J. (1992) *Proc. Natl. Acad. Sci. U.S.A. 89*, 6653−6657.

Perrouault, L., Asseline, U., Rivalle, C., Thuong, N. T., Bisagni, E., Giovannangeli, C., Le Doan, T., & Hélène, C. (1990) *Nature 344*, 358−360.

Pilch, D. S., Levenson, C., & Shafer, R. H. (1990) *Proc. Natl. Acad. Sci. U.S.A. 87*, 1942−1946.

Pilch, D. S., Martin, M.-T., Nguyen, C.-H., Sun, J.-S., Bisagni, E., Garestier, T., & Hélène, C. (1993a) *J. Am. Chem. Soc. 115*, 9942−9951.

Pilch, D. S., Waring, M. J., Sun, J.-S., Rougée, M., Nguyen, C.-H., Bisagni, E., Garestier, T., & Hélène, C. (1993b) *J. Mol. Biol. 232*, 926−946.

Pilch, D. S., Kirolos, M. A., Liu, X., Plum, G. E., & Breslauer, K. J. (1995) *Biochemistry 34*, 9962−9976.

Portugal, J., & Waring, M. J. (1986) *Nucleic Acids Res. 14*, 8735−8754.

Portugal, J., & Waring, M. J. (1987) *Eur. J. Biochem. 167*, 281−289.

Record, M. T., Jr., Woodbury, C. P., & Lohman, T. M. (1976) *Biopolymers 15*, 893−915.

Record, M. T., Jr., Anderson, C. F., & Lohman, T. M. (1978) *Q. Rev. Biophys. 11*, 103−178.

Riley, M., Maling, B., & Chamberlin, M. J. (1966) *J. Mol. Biol. 20*, 359−389.

Scaria, P. V., & Shafer, R. H. (1991) *J. Biol. Chem. 266*, 5417−5423.

Schmitz, H. U., & Hübner, W. (1993) *Biophys. Chem. 48*, 61−74.

Shafer, R. H., Yoshida, M., Banville, D. L., & Hu, S. (1990) in *Molecular Basis of Specificity in Nucleic Acid-Drug Interactions* (Pullman, B., & Jortner, J., Eds.) pp 59−65, Kluwer Academic Publishers, Dordrecht, The Netherlands.

Sun, J.-S., Lavery, R., Chomilier, J., Zakrzewska, K., Montenay-Garestier, T., & Hélène, C. (1991) *J. Biomol. Struct. Dyn. 9*, 425−436.

Thuong, N. T., & Hélène, C. (1993) *Angew. Chem., Int. Ed. Engl. 32*, 666−690.

Umemoto, U., Sarma, M. H., Gupta, G., Luo, J., & Sarma, R. H. (1990) *J. Am. Chem. Soc. 112*, 4539−4545.

Waring, M. J. (1974) *Biochem. J. 143*, 483−486.

Wells, R. D., Collier, D. A., Hanvey, J. C., Shimizu, M., & Wohlrab, F. (1988) *FASEB J. 2*, 2939−2949.

Wilson, W. D., Wang, Y.-H., Krishnamoorthy, C. R., & Smith, J. C. (1985) *Biochemistry 24*, 3991−3999.

Wilson, W. D., Tanious, F. A., Mizan, S., Yao, S., Kiselyov, A. S., Zon, G., & Strekowski, L. (1993) *Biochemistry 32*, 10614−10621.

Wiseman, T., Williston, S., Brandts, J. F., & Lin, L.-N. (1989) *Anal. Biochem. 179*, 131−137.

Yoshida, M., Banville, D. L., & Shafer, R. H. (1990) *Biochemistry 29*, 6585−6592.

BI9518609